Air-water CO_2 evasion from U.S. East Coast estuaries

Goossens, Nicolas[1], Laruelle, Goulven Gildas[1*], Arndt, Sandra[2], Cai, Wei-Jun[3] & Regnier, Pierre[1]

1 Department Geosciences, Environment and Society, Université Libre de Bruxelles, Brussels, Belgium
2 School of Geographical Sciences, University of Bristol, Bristol, UK
3 School of Marine Science and Policy, University of Delaware, Newark, Delaware, USA

*corresponding author: goulven.gildas.laruelle@ulb.ac.be

Abstract:

This study presents the first regional-scale assessment of estuarine CO_2 evasion along the East coast of the US (25 – 45 °N). The focus is on 43 tidal estuaries, which together drain a catchment of 697000 km^2 or 76 % of the total area within this latitudinal band. The approach is based on the Carbon – Generic Estuarine Model (C-GEM) that allows simulating hydrodynamics, transport and biogeochemistry for a wide range of estuarine systems using readily available geometric parameters and global databases of seasonal climatic, hydraulic, and riverine biogeochemical information. Our simulations, performed using conditions representative of the year 2000, suggest that, together, US East coast estuaries emit 1.9 TgC yr^{-1} in the form of CO_2, which correspond to about 40 % of the carbon inputs from rivers, marshes and mangroves. Carbon removal within estuaries results from a combination of physical (outgassing of supersaturated riverine waters) and biogeochemical processes (net heterotrophy and nitrification). The CO_2 evasion and its underlying drivers show important variations across individual systems, but reveal a clear latitudinal pattern characterized by a decrease in the relative importance of physical over biogeochemical processes along a North-South gradient. Finally, the results reveal that the ratio of estuarine surface area to the river discharge, S/Q (which has a scale of per meter discharged water per year), could be used as a predictor of the estuarine carbon processing in future regional and global scale assessments.

Deleted: 10^3

Formatted: Superscript

Deleted: Together

Formatted: Subscript

1 Introduction

Carbon fluxes along the land-ocean aquatic continuum are currently receiving increasing attention because of their recently recognized role in the global carbon cycle and anthropogenic CO_2 budget (Bauer et al., 2013; Regnier et al., 2013a; LeQuéré et al., 2014, 2015). Estuaries are important reactive conduits along this continuum, which links the terrestrial and marine global carbon cycles (Cai, 2011). Large amounts of terrestrial carbon transit through these systems, where they mix with carbon from autochthonous, as well as marine sources. During estuarine transit, heterotrophic processes degrade a fraction of the allochthonous and autochthonous organic carbon inputs, supporting a potentially significant, yet poorly quantified CO_2 evasion flux to the atmosphere. Recent estimates suggest that 0.15-0.25 PgC yr^{-1} is emitted from estuarine systems worldwide (Borges and Abril, 2012; Cai, 2011; Laruelle et al., 2010; Regnier et al., 2013a; Laruelle et al., 2013, Bauer et al., 2013). Thus, in absolute terms the global estuarine CO_2 evasion corresponds to about 15% of the open ocean CO_2 uptake despite the much smaller total surface area.

Currently, estimates of global estuarine CO_2 emissions are mainly derived on the basis of data-driven approaches that rely on the extrapolation of local measurements (Cai, 2011; Chen et al., 2013; Laruelle et al., 2013). While these approaches provide useful first-order estimates, they fail to capture the spatial and temporal heterogeneity of the estuarine environment (Bauer et al., 2013). In addition, these global estimates are biased towards anthropogenically influenced estuarine systems located in industrialized countries (Regnier et al., 2013a) and do not provide insights into the complex and dynamic interplay of biogeochemical and physical processes that controls estuarine CO_2 fluxes. However, Reaction transport models (RTMs) allow, in conjunction with data, the investigation of the estuarine response over the entire spectrum of fluctuating forcing conditions, including the long-term effect of land-use and climate changes (Bauer et al., 2013; Paerl et al., 2006; Thieu et al., 2010). In addition, RTMs can fully resolve the dynamic interplay of transport and transformation processes that control CO_2 fluxes across the entire estuarine gradient and at a high temporal and spatial resolution (Arndt et al., 2009; Arndt et al., 2011; Vanderborght et al., 2002;

Deleted: .

Deleted: Furthermore, observation-based approaches

Deleted: In this respect, integrated model-data approaches provide a suitable alternative.

Volta et al., 2014). Such models have recently been successfully applied to quantify system-wide, integrated biogeochemical indicators, such as Net Ecosystem Metabolism (Volta et al., 2014), carbon and nutrients budgets (Soetaert and Herman, 1995; Vanderborght et al., 2002; Billen et al., 2009; Laruelle et al., 2009) or nutrient filtering capacities (Arndt et al., 2009). To our knowledge, however, published modeling studies dedicated to quantifying estuarine CO_2 dynamics remain limited to the Scheldt estuary in Belgium-The Netherlands (Hofmann et al., 2008; Vanderborght et al., 2002) and to the Elbe in Germany (Volta et al., 2016a). Recently, Regnier et al., (2013b) quantified the contribution of different biogeochemical processes for CO_2 air-water fluxes in an idealized, funnel-shaped estuary forced by typical summer conditions characterizing a temperate Western European climate. Volta et al. (2016b) further investigated the effect of estuarine geometry on the CO_2 outgassing using three idealized systems. The Carbon Generic Estuarine Model (C-GEM, Volta et al., 2014) used for these studies can be applied to any temperate tidal estuary with little data demand. Using C-GEM, Volta et al. (2016a) established the first regional carbon budget for estuaries surrounding the North Sea by explicitly simulating the six largest systems of the area. Yet, local and regional quantifications of estuarine CO_2 fluxes using such an integrated data-RTM approach remain extremely limited and a RTM-based global quantification of estuarine CO_2 fluxes is currently lacking. The global quantification of the estuarine filter thus remains ignored in modelling efforts because terrestrial models representing the river network typically do not account for the estuaries (i.e. GLOBALNEWS: Seitzinger et al., 2005; Mayorga et al., 2010; SPARROW: Schwarz et al., 2006) and the spatial resolution of most continental shelf models not do yet allow representing estuaries other than the largest ones (Hofmann et al., 2011).

Here, an extended version of C-GEM (v1.0) is applied to quantify CO_2 exchange fluxes, as well as the overall organic and inorganic carbon budgets for the full suite of estuarine systems located along the entire East coast of the United States. The applied RTM approach allows to evaluate the relative significance of different physical and biogeochemical processes for the regional-scale CO_2 evasion within the ensemble of estuarine filters along the selected coastal segment, which is one of the most

Deleted: Integrated model-data approaches thus have the potential to significantly advance our mechanistic and quantitative understanding of global estuarine CO_2 fluxes, as well as their response to global change. RTMs

Formatted: Font: Not Bold, Not Italic, No underline

Deleted: a similar approach

Formatted: Font: Not Bold, Not Italic, No underline

Formatted: Font: Not Bold, Not Italic, No underline

Deleted: The lack of regional or global evaluations of the estuarine carbon dynamics can be partly explained by the high computational costs of RTM simulations. In addition, significant data requirements, such as comprehensive bathymetric and geometric information and boundary conditions may further limit the applicability of RTMs on a regional or global scale, while the need for benchmarking on a number of extensively surveyed, representative systems provides additional constraints. In attempt to overcome these constraints, the Carbon-Generic Estuary Model (C-GEM; Volta et al., 2014) has been developed with the aim of enabling the quantification of biogeochemical dynamics in estuaries on a regional and global scale. The focus is on tidal systems as defined by Dürr et al. (2011) and the approach is based on a one-dimensional, time-dependent representation of hydrodynamic, transport and reaction processes within an estuary. C-GEM is computationally efficient and reduces data requirements by using an idealized representation of the geometry to support the hydrodynamic calculations and, subsequently, transport and biogeochemical reaction processes. The C-GEM modeling platform thus enables hundreds to thousands of steady state or fully transient simulations spanning years to decades for a multitude of estuarine systems, using geometric information readily available through maps or remote sensing images. Despite the geometric simplification, C-GEM resolves the most important temporal and spatial scales characterizing the estuarine dynamics and provides an accurate description of the hydrodynamics, transport and biogeochemistry in tidal estuaries (Volta et al., 2014).¶

intensively monitored regions in the world. A unique set of regional data, including river and continental shelf sea partial pressure of CO_2 (pCO_2; Signorini et al., 2013; Laruelle et al., 2015), riverine biogeochemical properties (Lauerwald et al., 2013), estuarine eutrophication status (Bricker et al., 2007) and estuarine morphology (NOAA, 1985) are available. These comprehensive data sets are complemented by local observations of carbon cycling and CO_2 fluxes in selected, individual estuarine systems (see Laruelle et al., 2013 for a review), making the East coast of the United States an ideal region for a first, fully explicit regional evaluation of CO_2 evasion resolving every major tidal estuary along the selected coastal segment. An extensive review of published local estimates of CO_2 fluxes in estuarine systems worldwide can be found in Laruelle et al. (2013). The scale addressed in the present study is unprecedented so far (> 3000 km of coastline) and covers a wide range of estuarine morphological features, climatic conditions, land-use and land cover types, as well as urbanization levels.

After a description of the model itself and of the dataset used to set up the simulations, a local validation is presented which includes salinity, pCO_2 and pH longitudinal profiles for two well monitored systems (the Delaware Bay and the Altamaha River Estuary). The yearly averaged rates of CO_2 exchange at the air-water interface simulated by the model for 13 individual estuaries are also compared with observed values reported in the literature. Next, regional scale simulations for 43 tidal estuaries of the eastern US coast provide seasonal and yearly integrated estimates of the Net Ecosystem Metabolism (NEM), CO_2 evasion and carbon filtering capacity, CFilt. Model results are then used to elucidate the estuarine biogeochemical behavior along the latitudinal transect encompassed by the present study (30-45° N). Finally, our results are used to derive general relationships between carbon cycling and CO_2 evasion, and readily available estuarine geometrical parameters.

Formatted: Font: Not Bold, Not Italic, No underline

Formatted: Font: Not Bold, Not Italic, No underline

Formatted: Font: Not Bold, Not Italic, No underline

2. Regional description and model approach

2.1 Observation-based carbon budget for the East coast of the United States

The study area covers the Atlantic coast of the United States (Fig.1), from the southern tip of Florida (25°N) to Cobscook Bay (45°N) at the US-Canada boundary. This area encompasses distinct climatic zones and land cover types and exhibits a variety of morphologic features (Fig. 1). The region can be subdivided into several sub-regions following a latitudinal gradient (Signorini et al., 2013). In this study, we define three sub-regions following the boundaries suggested by the COSCAT segmentation (Meybeck et al., 2006; Laruelle et al., 2013) and the further subdivision described in Laruelle et al. (2015). From North to South, the regions are called North Atlantic, Mid Atlantic and South Atlantic Regions (Fig. 1). Total carbon inputs from watersheds to US East coast estuaries (Tab. 1) have been estimated to range from 4.0 to 10.7 Tg C yr^{-1} (Mayorga et al., 2010; Shih et al., 2010; Stets and Strieg, 2012; Tian et al., 2010; Tian et al., 2012), consisting of dissolved organic carbon (DOC; ~50%), dissolved inorganic carbon (DIC; ~40%) and particulate organic carbon (POC; ~10%). In addition, a statistical approach has been applied to estuaries of the region to quantify organic carbon budgets and Net Ecosystem Productivity (NEP) using empirical models (Herrmann et al., 2015).

Recent studies estimated that, along the East coast of the United States, rivers emit 11.4 TgC yr^{-1} of CO_2 to the atmosphere (Raymond et al., 2013), while continental shelf waters absorb between 3.4 and 5.4 TgC yr^{-1} of CO_2 from the atmosphere (Signorini et al., 2013). A total of thirteen local, annual mean estuarine CO_2 flux estimates across the air-water interface based on measurements are also reported in the literature and are grouped along a latitudinal gradient (Tab. 2). Four of these estimates are located in the South Atlantic region (SAR): Sapelo Sound, Doboy Sound, Altamaha Sound (Jiang et al., 2008), and the Satilla River estuary (Cai and Wang, 1998). Three studies investigate CO_2 fluxes in the mid-Atlantic Region (MAR): the York River Estuary (Raymond et al., 2000) and the Hudson River (Raymond et al., 1997). There is also a comprehensive CO_2 flux study for the Delaware Estuary published after the completion of this work (Joeseof et al., 2015). Six systems

Deleted: Figure

Deleted: ure

Deleted: Table

Deleted: fig

Deleted: 1

196 are located in the North Atlantic region (NAR): The Great Bay, the Little Bay, the Oyster estuary, the
197 Bellamy estuary, the Cocheco estuary (Hunt et al., 2010; 2011), and the Parker River estuary
198 (Raymond and Hopkinson, 2003). The mean annual flux per unit area from these local studies is
199 11.7±13.1 mol C m^{-2} yr^{-1} and its extrapolation to the total estuarine surface leads to a regional CO_2
200 evasion estimate of 3.8 Tg C y^{-1}. This estimate is in line with that of Laruelle et al. (2013) for the same
201 region which proposes an average CO_2 emission rate of 10.8 mol C m^{-2} yr^{-1}. Thus, CO_2 outgassing
202 could remove 35% to 95% of the riverine carbon loads during estuarine transit. About 75 % of the
203 air-water exchange occurs in tidal estuaries (2.8 Tg C y^{-1}) while lagoons and small deltas contribute to
204 the remaining 25 %. Although these simple extrapolations from limited observational data are
205 associated with large uncertainties, they highlight the potentially significant contribution of estuaries
206 to the CO_2 outgassing in the region. However, process-based quantifications of regional organic and
207 inorganic C budgets including air-water CO_2 fluxes for the estuarine systems along the East coast are
208 not available.

209 **2.2 Selection of estuaries**

210 The National Estuarine Eutrophication Assessment (NEAA) survey (Bricker et al., 2007), which uses
211 geospatial data from the National Oceanic and Atmospheric Administration (NOAA) Coastal
212 Assessment Framework (CAF) (NOAA, 1985), was used to identify and characterize 58 estuarine
213 systems discharging along the Atlantic coast of the United States. From this set, 43 'tidal' estuaries,
214 defined as a river stretch of water that is tidally influenced (Dürr et al., 2011), were retained (Fig. 1)
215 to be simulated by the C-GEM model, which is designed to represent such systems. Using outputs
216 from terrestrial models (Hartmann et al., 2009; Mayorga et al., 2010), the cumulated riverine carbon
217 loads for all the non-tidal estuaries that are excluded from the present study amount to 0.9 Tg C yr^{-1},
218 which represents less than 15% of the total riverine carbon loads of the region. These 15 systems are
219 located in the SAR (10) and in the MAR (5).

Deleted: 64

Deleted: 47

Deleted:

Deleted: fig

Formatted: Font: Not Bold, Not Italic, No underline

Deleted: The 15

Formatted: Font: Not Bold, Not Italic, No underline

Formatted: Font: Not Bold, Not Italic, No underline

Deleted: and account for less than 15% of the total riverine carbon loads of the region

The northeastern part of the domain (NAR, Fig. 1; Tab. 1) includes 20 estuaries along the Gulf of Maine and the Scotian shelf, covering a cumulative surface area of ~5300 km². It includes drowned valleys, rocky shores and a few tidal marshes. The climate is relatively cold (annual mean= 8°C) and the human influence is relatively limited because of low population density and low freshwater inputs. The mean estuarine water depth is 12.9 m and the mean tidal range is 2.8 m.

The central zone (MAR) includes 17 tidal estuaries accounting for a total surface area of 14500 km². The Chesapeake Bay and the Delaware estuaries alone contribute more than 60% to the surface area of the region. In this region, estuaries are drowned valleys with comparatively high river discharge and intense exchange with the ocean. Several coastal lagoons, characterized by a limited exchange with the ocean are located here, but are not included in our analysis. The Mid-Atlantic Region (MAR) is characterized by a mean annual temperature of 13°C and is strongly impacted by human activities, due to the presence of several large cities (e.g. New York, Washington, Philadelphia, Baltimore) and intense agriculture. The mean water depth is about 4.7 m and the tidal range is 0.8 m.

The southern Atlantic region (SAR) includes 10 tidal estuaries covering a total surface area of 12182 km². These systems are generally dendritic and surrounded by extensive salt marshes. The climate is subtropical with an average annual temperature of 19°C. Land use includes agriculture and industry, but the population density is generally low. Estuarine systems in the SAR are characterized by a shallow mean water depth of 2.9 m and a tidal range of 1.2 m.

2.3 Model set-up

The generic 1D Reactive-Transport Model (RTM) C-GEM (Volta et al., 2014) is used to quantify the estuarine carbon cycling in the 43 systems considered in this study. The approach is based on idealized geometries (Savenije, 2005; Volta et al., 2014) and is designed for regional and global scale applications (Regnier et al., 2013b; Volta et al., 2014, 2016a). The model approach builds on the premise that hydrodynamics exerts a first-order control on estuarine biogeochemistry (Arndt et al.,

Deleted: table

Deleted: 47

2007; Friedrichs and Hofmann, 2001) and CO_2 fluxes (Regnier et al., 2013a). The method takes advantage of the mutual dependence between geometry and hydrodynamics in tidal estuaries (Savenije, 1992) and the fact that, as a consequence, transport and mixing can be easily quantified from readily available geometric data (Regnier et al., 2013a; Savenije, 2005; Volta et al., 2016b).

2.3.1 Description of idealized geometries for tidally-averaged conditions

Although tidal estuaries display a wide variety of shapes, they nevertheless share common geometric characteristics that are compatible with an idealized representation (Fig. 2, Savenije, 1986; Savenije, 2005). For tidally-averaged conditions, their width B (or cross-sectional area A) can be described by an exponential decrease as a function of distance, *x*, from the mouth (Savenije, 1986; Savenije, 2005):

$$B = B0 * \exp\left(-\frac{x}{b}\right) \quad (1)$$

where B (m) is the tidally averaged width, B0 (m) the width at the mouth, x (m) the distance from the mouth (x=0) and b (m) the width convergence length (Fig. 2). The width convergence length, b, is defined as the distance between the mouth and the point at which the width is reduced to B0 e^{-1}. It is directly related to the dominant hydrodynamic forcing. A high river discharge typically results in a prismatic channel with long convergence length (river dominated estuary), while a large tidal range results in a funnel-shaped estuary with short convergence length (marine dominated estuary). At the upstream boundary, the estuarine width is given by:

$$B_L = B0 * \exp\left(-\frac{L}{b}\right) \quad (2)$$

Where L denotes the total estuarine length (m) along the estuarine longitudinal axis.

The total estuarine surface S (m^2) can be estimated by integrating equation (1) over the estuarine length:

$$S = \int_0^L B\,dx = b * B0 * \left(1 - \exp\left(-\frac{L}{b}\right)\right) \quad (3)$$

The width convergence length is then calculated from B0, B_L, L and the real estuarine surface area (SR) by inserting equation (2) in equation (3):

$$b = \frac{SR}{B0 - BL} \quad (4)$$

SR is calculated for each system using the SRTM water body data (Fig. 3a), a geographical dataset encoding high-resolution worldwide coastal outlines in a vector format (NASA/NGA, 2003). While such a database exists for a well monitored region such as the East coast of the US, resorting to using the idealized estuarine surface area (S) is necessary in many other regions. The longitudinal mean, tidally averaged, depth h (m), is obtained from the National Estuarine Eutrophication Assessment database (Bricker et al., 2007).

Using this idealized representation, the estuarine geometry can be defined by a limited number of parameters: the width at the mouth (B_0), the estuarine length (L), the estuarine width at the upstream limit (B_L) and the mean depth h. These parameters can be easily determined from local maps or Google Earth using Geographic Information Systems (GIS) or obtained from databases (NASA/NGA, 2003).

2.3.2 Hydrodynamics, transport and biogeochemistry

Estuarine hydrodynamics are described by the one-dimensional barotropic, cross-sectionally integrated mass and momentum conservation equations for a channel with arbitrary geometry (Nihoul and Ronday, 1976; Regnier et al., 1998; Regnier and Steefel, 1999):

$$r_s \frac{\partial A}{\partial t} + \frac{\partial Q}{\partial x} = 0 \quad (5)$$

Deleted: fig

Formatted: Font: Not Bold, Not Italic, No underline

Formatted: Font: Not Bold, Not Italic, No underline

Deleted: through GIS, local maps, Google Earth

Deleted: is

$$\frac{\partial U}{\partial t} + U\frac{\partial U}{\partial x} = -g\frac{\partial \zeta}{\partial x} - g\frac{U|U|}{C_z^2 H} \quad (6)$$

Deleted: $\frac{\partial U}{\partial t} + U\frac{\partial U}{\partial x} = -$

where:

t	time	[s]
x	distance along the longitudinal axis	[m]
A	cross-section area $A = H \cdot B$	[m^2]
Q	cross-sectional discharge $Q = A \cdot U$	[$m^3\ s^{-1}$]
U	flow velocity Q / A	[$m\ s^{-1}$]
r_s	storage ratio $r_s = B_s / B$	[-]
B_s	storage width	[m]
g	gravitational acceleration	[$m\ s^{-2}$]
ξ	elevation	[m]
H	total water depth $H = h + \xi(x,t)$	[m]
C_z	Chézy coefficient	[$m^{1/2}\ s^{-1}$]

Formatted: Subscript

The coupled partial differential equations (Eqs. (5) and (6)) are solved by specifying the elevation $\xi_0(t)$ at the estuarine mouth and the river discharge $Q_r(t)$ at the upstream limit of the model domain.

Deleted: 6

Deleted: 7

The one-dimensional, tidally-resolved, advection-dispersion equation for a constituent of concentration $C(x,t)$ in an estuary can be written as (e.g. Pritchard, 1958):

$$\frac{\partial C}{\partial t} + \frac{Q}{A}\frac{\partial C}{\partial x} = \frac{1}{A}\frac{\partial}{\partial x}\left(AD\frac{\partial C}{\partial x}\right) + P \quad (7)$$

where $Q(x,t)$ and $A(x,t)$ denote the cross-sectional discharge and area, respectively and are provided by the hydrodynamic model (eq. 5 and 6). $P(x,t)$ is the sum of all production and consumption process rates affection the concentration of the constituent. The effective dispersion coefficient D ($m^2\ s^{-1}$) implicitly accounts for dispersion mechanisms associated to sub-grid scale processes (Fischer, 1976; Regnier et al., 1998). In general, D is maximal near the sea, decreases upstream and becomes virtually zero near the tail of the salt intrusion curve (Preddy, 1954; Kent, 1958; Ippen and Harleman, 1961; Stigter and Siemons, 1967). The effective dispersion at the estuarine mouth can be quantified by the following relation (Savenije, 1986):

$$D_0 = 26 \cdot (h_0)^{1.5} \cdot (N \cdot g)^{0.5} \quad (8)$$

where h_0 (m) is the tidally-averaged water depth at the estuarine mouth and N is the dimensionless Canter Cremers' estuary number defined as the ratio of the freshwater entering the estuary during a tidal cycle to the volume of salt water entering the estuary over a tidal cycle (Simmons, 1955).

$$N = \frac{Q_b \cdot T}{P} \quad (9)$$

In this equation, Q_b is the bankfull discharge ($m^3\ s^{-1}$), T is the tidal period (s) and P is the tidal prism (m^3). For each estuary, N can thus be calculated directly from the hydrodynamic model. The variation in D along the estuarine gradient can be described by Van der Burgh's equation (Savenije, 1986):

$$\frac{\partial D}{\partial x} = -K \frac{Q_r}{A} \quad (10)$$

where K is the dimensionless Van der Burgh's coefficient and the minus sign indicates that D increases in downstream direction (Savenije, 2012). The Van der Burgh's coefficient is a shape factor that has values between 0 and 1 (Savenije, 2012), and is a function of estuarine geometry for tidally average conditions. Therefore, each estuarine system has its own characteristic K value, which correlates with geometric and hydraulic scales (Savenije, 2005). Based on a regression analysis

Deleted: 6
Deleted: 7
Deleted: Van der Burgh
Deleted: 1972
Formatted: Font: Not Bold, Not Italic, No underline
Deleted: 9

346 covering a set of 15 estuaries, it has been proposed to constrain *K* from the estuarine geometry
347 (Savenije, 1992):

348 $$K = 4.32 \cdot \frac{h_0^{0.36}}{B_0^{0.21} \cdot b^{0.14}} \quad \text{with} \quad 0 < K < 1 \qquad (11)$$

349 Reaction processes *P* considered in C-GEM comprise aerobic degradation, denitrification,
350 nitrification, primary production, phytoplankton mortality and air-water gas exchange for O_2 and CO_2
351 (Fig. 4 and Tab. 3). These processes and their mathematical formulation are described in detail in
352 Volta et al. (2014) and Volta et al. (2016a).

353 The non-linear partial differential equations for the hydrodynamics are solved by a finite difference
354 scheme following the approach of (Regnier et al., 1997; Regnier and Steefel, 1999) and
355 (Vanderborght et al., 2002). The timestep Δt is 150s and the grid size Δx is constant along the
356 longitudinal axis of the estuary. The grid size default value is 2000 m, but can be smaller for short
357 length estuaries to guarantee a minimum of 20 grid points within the computational domain.
358 Transport and reaction terms are solved in sequence within a single timestep using an operator
359 splitting approach (Regnier et al., 1997). The advection term in the transport equation is integrated
360 using a third-order accurate total variation diminishing (TVD) algorithm with flux limiters (Regnier et
361 al., 1998), ensuring monotonicity (Leonard, 1984), while a semi-implicit Crank-Nicholson algorithm is
362 used for the dispersion term (Press et al., 1992). These schemes have been extensively tested using
363 the CONTRASTE estuarine model (e.g. Regnier et al., 1998; Regnier and Steefel, 1999; Vanderborght
364 et al., 2002) and guarantee mass conservation to within <1%. The reaction network (including
365 erosion-deposition terms when the constituent is a solid species), is numerically integrated using the
366 Euler method (Press et al., 1992). The primary production dynamics, which requires vertical
367 resolution of the photic depth, is calculated according to the method described in Vanderborght et
368 al. (2007). This method assumes an exponential decrease of the light in the water column (Platt et
369 al., 1980), which is solved using a Gamma function.

Deleted: 10
Deleted: Table
Deleted: 2
Deleted:)
Deleted: ,
Deleted: (

2.4 Boundary and forcing conditions

Boundary and forcing conditions are extracted from global databases and global model outputs that are available at 0.5° resolution. Therefore, C-GEM simulations are performed at the same resolution according to the following procedure. First, 43 coastal cells corresponding to tidal estuaries are identified in the studied area (Fig. 1). If the mouth of an estuary is spread over several 0.5° grid cells, those cells are regrouped in order to represent a single estuary (e.g. Delaware estuary), and subsequently, a single idealized geometry is defined as described above. The model outputs (Hartmann et al. , 2009; Mayorga et al., 2010) and databases (Antonov et al., 2010; Garcia et al., 2010a; Garcia et al., 2010b) used to constrain our boundary conditions are representative of the year 2000.

For each resulting cell, boundary and forcing conditions are calculated for the following periods: January-March; April-June; July-September and October-December. This allows for an explicit representation of the seasonal variability in the simulations.

2.4.1 External forcings

Transient physical forcings are calculated for each season and grid cell using monthly mean values of water temperature (World Ocean Atlas, 2009) and seasonal averaged values for wind speed (Cross-Calibrated-Multi-Platform (CCMP) Ocean Surface Wind Vector Analyses project (Atlas et al., 2011)). Mean daily solar radiation and photoperiods (corrected for cloud coverage using the ISCCP Cloud Data Products, Rossow and Schiffer, 1999) are calculated depending on latitude and day of the year using a simple model (Brock, 1981).

2.4.2 Riverine discharge, concentrations and fluxes

River discharges are extracted from the UNH/GRDC runoff dataset (Fekete et al., 2002). These discharges represent long-term averages (1960-1990) of monthly and annual runoff at 0.5 degree resolution. The dataset is a composite of long-term gauging data, which provides average runoff for

Deleted: 47

Deleted: fig

Formatted: Font: Not Bold, Not Italic, No underline

the largest river basins, and a climate driven water balance model (Fekete et al., 2002). Total runoff values are then aggregated for each watershed at the coarser 0.5 degree resolution (Fig. 3b). Next, seasonal mean values (in m^3 s^{-1}) are derived in order to account for the intra-annual variability in water fluxes. Based on annual carbon and nutrients inputs from the watersheds (Mg y^{-1}), mean annual concentrations (mmol m^{-3}) are estimated for each watershed using the UNH/GRDC annual runoff (km^3 y^{-1}). Mean seasonal concentrations are then calculated from the seasonally resolved river water fluxes of a given sub-region.

Deleted: fig

Annual inputs of dissolved organic carbon (DOC), particulate organic carbon (POC) and inorganic nutrients are derived from the globalNEWS2 model (Mayorga et al., 2010). Global NEWS is a spatially explicit, multi-element (N, P, Si, C) and multi-form global model of nutrient exports by rivers. In a nutshell, DOC exports are a function of runoff, wetland area, and consumptive water use (Harrison et al., 2005). No distinction is made between agricultural and natural landscapes, since they appear to have similar DOC export coefficients (Harrison et al., 2005). Sewage inputs of OC are ignored in GlobalNEWS, because their inclusion did not improve model fit to data (Harrison et al., 2005). POC exports from watersheds are estimated using an empirical relationship with Suspended Particulate Matter (SPM; Ludwig et al., 1996). Inorganic nitrogen (DIN) and phosphorus (DIP) fluxes calculated by GlobalNEWS depend on agriculture and tropical forest coverage, fertilizer application, animal grazing, sewage input, atmospheric N deposition and biological N fixation (Mayorga et al., 2010). The inputs of dissolved silica (DSi) are controlled by soil bulk density, precipitation, slope, and presence of volcanic lithology (Beusen et al., 2009).

The DIN speciation is not provided by the GlobalNEWS2 model. The NH_4 and NO_3 concentrations are therefore determined independently on the basis of an empirical relationship between ammonium fraction (NH4/DIN ratio) and DIN loads (Meybeck, 1982). Dissolved Oxygen (DO) concentrations are extracted from the water quality criteria recommendations published by the United States Environmental Protection Agency (EPA, 2009). The same source is used for phytoplankton

concentrations, using a chlorophyll-a to phytoplankton carbon ratio of 50 gC (gChla)$^{-1}$ (Riemann et al., 1989) to convert the EPA values to carbon units used in the present study.

Inputs of dissolved inorganic carbon (DIC) and total Alkalinity (ALK) are calculated from values reported in the GLORICH database (Hartmann et al., 2009). For each watershed, seasonal mean values of DIC and ALK concentrations are estimated from measurements performed at the sampling locations that are closest to the river-estuary boundary. The spatial distribution of annual inputs of TOC=DOC+POC, DIC, and TC=TOC+DIC from continental watersheds to estuaries are reported in Fig. 5a, 5c and 5d, respectively. The contribution of tidal wetlands to the TOC inputs is also shown (Fig. 5b). Overall, the TC input over the entire model domain is estimated at 4.6 Tg C yr^{-1}, which falls in the lower end of previous reported estimations (Najjar et al. 2012).

Deleted: fig

2.4.3 Inputs from tidal wetlands

The DOC input of estuarine wetlands (Fig. 5b) scales to their fraction, W, of the total estuarine and is calculated using the GlobalNEWS parameterization:

Formatted: Font: Not Bold, Not Italic, No underline

Deleted: their surface area W

$$Y\_DOC = \frac{\left[(E\_C_{wet} * W) + E\_C_{dry} * (1 - W)\right] * R^a * Q_{act}}{Q_{nat}} \quad (12)$$

Deleted: 11

$$\frac{Y\_DOC_{wet}}{Y\_DOC} = \frac{E\_C_{wet} * W}{E\_C_{wet} * W + E\_C_{dry} * (1 - W)} \quad (13)$$

Deleted: 12

where Y_DOC is the DOC yield (kg C km^{-2} y^{-1}) calculated for the entire watershed, Y_DOC$_{wet}$ is the estimated DOC yield from wetland areas (kg C km^{-2} y^{-1}), Q_{act}/Q_{nat} is the ratio between the measured discharge after dam construction and before dam construction, E_C$_{wet}$ and E_C$_{dry}$ (kg C km^{-2} y^{-1}) are the export coefficients of DOC from wetland and non-wetland soils, respectively. W is the

percentage of the land area within a watershed that is covered by wetlands, R is the runoff (m y^{-1}) and α is a unit-less calibration coefficient defining how non-point source DOC export responds to runoff. The value of a is set to 0.95, consistent with the original GlobalNEWS -DOC model of Harrison et al. (2005). The carbon load Y_DOC_{wet} is then exported as a diffuse source along the relevant portions of estuary. The estuarine segments receiving carbon inputs from tidal wetlands are identified using the National Wetlands Inventory of the U.S. Fish and Wildlife Service (U.S. Fish and Wildlife Service, 2014). The inputs from those systems are then allocated to the appropriate grid cell of the model domain using GIS. The flux calculated is an annual average that is subsequently partitioned between the four seasons as a function of the mean seasonal temperature, assumed to be the main control of the wetland-estuarine exchange. This procedure reflects the observation that in spring and early summer, DOC export is small as a result of its accumulation in the salt marshes induced by the high productivity (Dai and Wiegert, 1996), (Jiang et al., 2008). In late summer and fall, the higher water temperature and greater availability of labile DOC contribute to higher bacterial remineralization rates in the intertidal marshes (Cai et al., 1999; Middelburg et al., 1996; Wang and Cai, 2004), which induce an important export. This marsh production-recycle-export pattern is consistent with the observed excess DIC signal in the offshore water (Jiang et al. 2013). DIC export from tidal wetlands is neglected here because it is assumed that OC is not degraded before reaching the estuarine realm. Although this assumption may lead to an overestimation of OC export from marshes and respiration in estuarine water, it will not significantly affect the water pCO_2 and degassing in the estuarine waters because mixing is faster than respiration.

2.4.4 Concentrations at the estuarine mouth

For each estuary, the downstream boundary is located 20 km beyond the mouth to minimize the bias introduced by the choice of a fixed concentration boundary condition to characterize the ocean water masses (e.g. Regnier et al., 1998). This approach also reduces the influence of marine boundary conditions on the simulated estuarine dynamics, especially for all organic carbon species

whose concentrations are fixed at zero at the marine boundary. This assumption ignores the intrusion of marine organic carbon into the estuary during the tidal cycle but allows focusing on the fate of terrigenous material and its transit through the estuarine filter. DIC concentrations are extracted from the GLODAP dataset (Key et al., 2004), from which ALK and pH are calculated assuming CO_2 equilibrium between coastal waters and the atmosphere. The equilibrium value is computed using temperature (WOA2009, Locarnini et al., 2010) and salinity (WOA2009, Antonov et al. (2010)) data which vary both spatially and temporally. The equilibrium approach is a reasonable assumption because differences in partial pressure ΔpCO_2 between coastal waters and the atmosphere are generally much smaller (0-250 µatm (Signorini et al., 2013)) than those reported for estuaries (ΔpCO_2 in the range 0-10000 µatm (Borges and Abril, 2012)). Salinity, DO, NO_3, DIP and DSi concentrations are derived from the World Ocean Atlas (Antonov et al., 2010; Garcia et al., 2010a; Garcia et al., 2010b). NH_4 concentrations are set to zero in marine waters. For all variables, seasonal means are calculated for each grid cell of the boundary.

Deleted:

Deleted: domain

2.5 Biogeochemical indicators

The model outputs (longitudinal profiles of concentration and reaction rates) are integrated in time over the entire volume or surface of each estuary to produce the following indicators of the estuarine biogeochemical functioning (Regnier et al., 2013b): the mean annual Net Ecosystem Metabolism (*NEM*), the air-water CO_2 flux (FCO_2), the carbon and nitrogen filtering capacity (*CFilt* and *NFilt*) and their corresponding element budgets. The *NEM* (molC y^{-1}) (Caffrey, 2004; Odum, 1956) is defined as the difference between net primary production (*NPP*) and total heterotrophic respiration (*HR*) at the system scale:

$$NEM = \int_0^{365} \int_0^{L} [NPP(x,t) - R_{aer}(x,t) - R_{den}(x,t)] * B(x) * H(x,t)\, dx\, dt \quad (14)$$

Deleted: 13

where *NPP* is the Net Primary Production (mol C m^{-3} y^{-1}), R_{aer} the aerobic degradation of organic matter (in mol C m^{-3} y^{-1}) and R_{den} the denitrification (in mol C m^{-3} y^{-1}) (see Volta et al., 2014 for detailed formulations). *NEM* is thus controlled by the production and decomposition of autochthonous organic matter, by the amount and degradability of organic carbon delivered by rivers and tidal wetlands and by the export of terrestrial and in-situ produced organic matter to the adjacent coastal zone. Following the definition of *NEM*, the trophic status of estuaries can be net heterotrophic (NEM<0) when *HR* exceeds *NPP* or net autotrophic (NEM>0), when *NPP* is larger than *HR* because the burial and export of autochthonous organic matter exceeds the decomposition of river-borne material.

The FCO_2 (mol C y^{-1}) is defined as:

$$FCO_2 = \int_0^{365} \int_0^{L} RCO_2(x,t) * B(x)\, dx\, dt \qquad (15)$$

Deleted: 14

$$RCO_2(x,t) = -\mathrm{v_p}(\mathrm{x,t})\left(\left[CO_{2(aq)}\right](x,t) - K_0(x,t) * P_{CO2}(x,t)\right) \qquad (16)$$

Deleted: 15

where RCO_2 (molC m^{-2} y^{-1}) is the rate of exchange in CO_2 at the air-water interface per unit surface area, v_p is the piston velocity (m y^{-1}) and is calculated according to Regnier et al. (2002) to account for the effect of current velocity and wind speed, [*CO2(aq)*] is the concentration of CO_2 in the estuary (mol m^{-3}), K_0 is Henry's constant of CO_2 in sea water (mol m^{-3} atm^{-1}) and P_{CO2} is the atmospheric partial pressure in CO_2 (atm).

The carbon filtering capacity (in %) corresponds to the fraction of the river-borne supply that is lost to the atmosphere and is defined here as the ratio of the net outgassing flux of CO_2 and the total inputs of C, e.g. total carbon expressed as the sum of inorganic and organic carbon species, both in the dissolved and particulate phases.

$$CFilt = \frac{FCO_2}{\int_0^{365} Q*[TC]_{riv}\, dt} * 100 \quad (17)$$

where $[TC]_{riv}$ denote the total concentrations of C in the riverine inputs.

Fluxes per unit area for FCO_2 and *NEM*, noted $\overline{FCO_2}$ and $\overline{NEM}$, respectively, are defined in mol C m^{-2} y^{-1} and are calculated by dividing the integrated values calculated above by the (idealized) estuarine surface *S*:

$$\overline{NEM} = \frac{NEM}{S} * 1000 \quad (18)$$

$$\overline{FCO_2} = \frac{FCO_2}{S} * 1000 \quad (19)$$

Seasonal values for the biogeochemical indicators are calculated using the same formula as above, but calculate the integral over a seasonal rather than annual timescale (i.e. 3 months).

2.6 Model-data comparison

C-GEM has been specifically designed for an application on a global/regional scale requiring the representation of a large number of individual and often data-poor systems. Maximum model transferability and minimum validation requirements were thus central to the model design process and the ability of the underlying approach in reproducing observed dynamics with minimal calibration effort has been extensively tested. The performance C-GEM's one-dimensional hydrodynamic and transport models using idealized geometries have been evaluated for a number of estuarine systems exhibiting a wide variety of shapes (Savenije, 2012). In particular, it has been shown that the estuarine salt intrusion can be successfully reproduced using the proposed modeling approach (Savenije 2005; Volta et al., 2014; 2016b). In addition, C-GEM's biogeochemistry has also been carefully validated for geometrically contrasting estuarine system in temperate climate zones.

Deleted: 16

Deleted: 17

Deleted: 18

Formatted: Font: Not Bold, Not Italic, No underline

Formatted: Font: Not Bold, Not Italic, No underline

Deleted: of 1D

Simulations for the Scheldt Estuary (Belgium and the Netherlands), a typical funnel-shaped estuary, were validated through model-data and model-model comparison (Volta et al., 2014; Volta et al., 2016a). Furthermore, simulations for the Elbe estuary (Germany), a typical prismatic shape estuary that drains carbonate terrains and, thus, exhibits very high pH was validated against field data (Volta et al., 2016a). In addition, C-GEM carbon budgets have been compared budget derived from observations for 6 European estuaries discharging in the North Sea (Volta et al., 2016a). Although C-GEM has been specifically designed and tested for the type of regional application presented here, its transferability from North Sea to US East Coast estuaries was further evaluated by assessing its performance in two East Coast estuaries. First, the hydrodynamic and transport model was tested for the Delaware Bay (MAR). The model was forced with the monthly, minimal and maximal observed discharge at Trenton over the period between 1912 and 1985 (UNH/GRDC Database, Fekete et al., 2000). Simulated salinity profiles are compared with salinity observations from January, February, May and June (the months with the highest number of data entries), which were extracted from the UNH/GRDC Database. Figure 6 shows that the model captures both the salinity intrusion length and the overall shape of the salinity profile well. In addition, the performance of the biogeochemical model and specifically its ability to reproduce pH and pCO_2 profiles was evaluated by a model-data comparison for both the Delaware Bay (MAR) in July 2003 and the Altamaha river estuary (SAR) in October 1995. Similar to Volta et al., 2016a, the test systems were chosen due to their contrasting geometries. The Delaware Bay is a marine dominated system characterized by a pronounced funnel shape, while the Altamaha River has a prismatic estuary characteristic of river dominated systems (Jiang et al., 2008). Monthly upstream boundary conditions for nutrients, as well as observed pH data and calculated pCO_2 are extracted from datasets described in (Sharp, 2010) and (Sharp et al., 2009) for the Delaware and in (Cai and Wang, 1998; Jiang et al., 2008) and (Cai et al., 1998) for the Altamaha river estuary. The additional forcings and boundary conditions are set similarly to the simulation for 2000 (see Tab. 2, 3, 4, 5, 6 in SI). Figure 7 shows that measured and simulated pH values are in good agreement with observed pH and observation-derived calculations

Deleted: Simulations

Deleted: draining

Deleted: resulting in

Deleted: to

Deleted: -based estimations

Formatted: Font: Not Bold, Not Italic, No underline

Formatted: Font: Not Bold, Not Italic, No underline

Formatted: Font: Not Bold, Not Italic

Formatted: Font: Not Bold, Not Italic, No underline

Formatted: Font: Not Bold, Not Italic, No underline

Formatted: Font: Not Bold, Not Italic, No underline

Formatted: Font: Not Bold, Not Italic, No underline

of pCO_2. In the Delaware Bay, a pH minimum is located around km 140 and is mainly caused by intense nitrification sustained by large inputs of NH_4 from the Philadelphia urban area, coupled to an intense heterotrophic activity. Both processes lead to a well-developed pCO_2 increase in this area (Fig. 7b). Although no pCO_2 data were available for validation for the period from which boundary conditions were extracted, the simulated profile agree with pCO_2 measurement from July 2013 presented by Joesoef et al. (2015) with pCO_2 values close to equilibrium with the atmosphere in the widest section of the Delaware Bay (close to the estuarine mouth) and values above 1200 µatm at salinities below 5. For the Altamaha river estuary, pH steadily increases from typical river to typical coastal ocean values (Fig. 7b). In addition, both observations and model results reveal that outgassing is very intense in the low-salinity region with more than a 5 fold decrease in pCO_2 between salinity 0 and 5 (Fig. 7d).

While such local validations allow assessing the performance of the model for a specific set of conditions, the purpose of this study is to capture the average biogeochemical behavior of the estuaries of the eastern coast of the US. Therefore, in addition to the system-specific validation, published annually averaged FCO_2 estimates for 13 tidal systems located within the study area collected over the 1994-2006 period are compared to simulated FCO_2 for conditions representative of the year 2000. Overall, simulated FCO_2 are comparable to values reported in the literature (Tab. 2). Although discrepancies, which sometimes can significant, are observed at the level of individual systems, the model captures remarkably well the overall trend in CO_2 evasion rate across estuaries. The model simulates low CO_2 efflux (< 5 mol C m^{-2} yr^{-1}) for the 7 systems were such conditions have been observed, while the 6 systems for which the CO_2 evasion exceeds 10 mol C m^{-2} yr^{-1} are the same in the observations and in the model runs. The discrepancy at the individual system level likely result from a combination of factors, including the choice of model processes and there parametrization, the uncertainties in constraining boundary conditions and the limited representability of instantaneous and local observed.

Formatted: Font: Not Bold, Not Italic, No underline

Formatted: Font: Not Bold, Not Italic, No underline

Formatted: Font: Not Bold, Not Italic, No underline

Deleted: This analysis is pursued here by evaluating our model results in the context of estuarine CO_2 evasion estimates along the East coast of the US.

3 Results and discussion

3.1 Spatial variability of estuarine carbon dynamics

Figure 8 presents the spatial distribution of simulated mean annual $\overline{FCO_2}$ and -$\overline{NEM}$ (Fig. 8a), as well as FCO_2 and -*NEM* (Fig. 8b). In general, mean annual $\overline{FCO_2}$ are about 30% larger than mean annual $\overline{NEM}$, with the exception of six estuaries situated in the North of the coastal segment. Overall, the $\overline{NEM}$ is characterized by smaller system to system variability compared to the $\overline{FCO_2}$ in all regions. In addition, Fig. 8 reveals distinct differences across the three coastal segments and highlights the important influence of the estuarine geometry and residence time, as well as the latitudinal temperature gradient on estuarine carbon cycling.

Overall, $\overline{FCO_2}$ values are the lowest in the NAR (mean flux = 17.3 ± 16.4 mol C m^{-2} y^{-1}; surface weighted average = 23.1 mol C m^{-2} y^{-1}), consistent with previously reported very low values for small estuaries surrounding the Gulf of Maine (Hunt et al., 2010; 2011; Tab. 2). In contrast, $\overline{NEM}$ reveals a regional minimum in the NAR (-51.2 ± 16.6 mol C m^{-2} y^{-1}; surface weighted average = -52.8 mol C m^{-2} y^{-1}). The MAR is characterized by intermediate values for $\overline{FCO_2}$, with a mean flux of 26.3 ± 34.6 mol C m^{-2} y^{-1} (surface weighted average =11.1 mol C m^{-2} y^{-1}) and lowest values for $\overline{NEM}$ (-15.1 ± 14.2 mol C m^{-2} y^{-1}; surface weighted average =-7.4 mol C m^{-2} y^{-1}). This region also shows the largest variability in CO_2 outgassing compared to the NAR and SAR, with the standard deviation exceeding the mean $\overline{FCO_2}$, and individual estimates ranging from 3.9 mol C m^{-2} y^{-1} to 150.8 mol C m^{-2} y^{-1}. This variability is mainly the result of largely variable estuarine surface areas and volumes. Some of the largest East coast estuaries (e.g. Chesapeake and Delaware Bays), as well as some of smallest estuaries (e.g. York River and Hudson River estuaries, Raymond et al., 1997; 2000), are located in this region (Tab. 2 and 4). The maximum values of 150.8 mol C m^{-2} y^{-1} simulated in the MAR are similar to the highest FCO_2 reported in the literature (132.3 mol C m^{-2} y^{-1} for the Tapti estuary in India; Sarma et al., 2012). The SAR is characterized by the highest mean $\overline{FCO_2}$ (46.7 ± 33.0 mol C m^{-2} y^{-1}; surface weighted average

Deleted: 6
Deleted: 6a
Deleted: 6
Deleted: Figure
Deleted: 6
Deleted: table
Deleted: 3
Deleted: maximum
Deleted: table
Deleted: 3

646 = 40.0 mol C m^{-2} y^{-1}) and intermediate $\overline{NEM}$ (-36.8 ± 24.7 mol C m^{-2} y^{-1}; surface weighted average = -
647 31.2 mol C m^{-2} y^{-1}).

648 The NAR is characterized by a regional minimum in $\overline{FCO_2}$, and only contributes 4.6% to the total
649 FCO_2 of the East coast of the US, owing to the small cumulative surface area available for gas
650 exchange in its 10 estuarine systems. In contrast, the 18 MAR estuaries, with their large relative
651 contribution to the total regional estuarine surface area, account for as much as 70.1% of the total
652 outgassing. Because of their smaller cumulated surface area compared to those of the MAR, the 14
653 SAR estuaries account for merely 25.3% of the total outgassing despite their regional maximal $\overline{FCO_2}$.
654 A similar, yet slightly less pronounced pattern emerges for the $\overline{NEM}$. The NAR, MAR and SAR
655 respectively contribute 13.7%, 60.7% and 25.6% to the total regional net ecosystem metabolism. The
656 comparatively larger relative contribution of the NAR to the total *NEM* as compared to the total
657 FCO_2 can be explained by the importance of the specific aspect ratio for NEM. A larger ratio of
658 estuarine width b0 and convergence length b corresponds to a more funnel shaped estuary while a
659 low ratio corresponds to a more prismatic geometry (Savenije, 2000; Volta et al., 2014). In the NAR,
660 estuaries are generally characterized by relatively narrow widths and deep-water depths, thus
661 limiting the potential surface area for gas exchange with the atmosphere. However, the relative
662 contribution of each region to the total regional *NEM* and FCO_2 is largely controlled by estuarine
663 surface area. Figure 9 illustrates the cumulative *NEM* (a) and FCO_2 (b) as a function of the cumulative
664 estuarine surface areas. The disproportionate contribution of large estuaries from the MAR
665 translates into a handful of systems (Chesapeake and Delaware Bays and the main tributaries of the
666 former, in particular) contributing to roughly half of the regional *NEM* and FCO_2, in spite of relatively
667 low individual rates per unit surface area. However, the smallest systems (mostly located in the NAR
668 and SAR) nevertheless still contribute a significant fraction to the total regional *NEM* and FCO_2. The
669 27 smallest systems merely account for less than 10% of the total regional estuarine surface area,
670 yet contribute 38% and 29% to the total regional *NEM* and FCO_2, respectively (Fig. 9). This

Deleted: more than 70%

Formatted: Font: Not Bold, Not Italic, No underline

Formatted: Font: Not Bold, Not Italic, No underline

Deleted: 7

Deleted: Figure

Deleted: 7

disproportioned contribution can be mainly attributed to their high individual $\overline{FCO_2}$ and $\overline{NEM}$. This is illustrated by the average simulated $\overline{FCO_2}$ for all 27 smallest systems (calculated as the sum of each estuarine CO_2 outgassing per unit surface area divided by the total number of estuarine systems) which is significantly higher (30.2 mol C m^{-2} y^{-1}) than its surface weighted average (14 mol C m^{-2} y^{-1}). Thereby accounting for the disproportionate contribution of very large systems (calculated as the sum of each estuarine CO_2 outgassing divided by the total estuarine surface area across the region).

Following the approach used in Regnier et al. (2013), the contribution of each biogeochemical process to *FCO₂* is assessed by evaluating their individual contribution to DIC and ALK changes taking into account the local buffering capacity of an ionic solution when TA and DIC are changing due to internal processes, but ignoring advection and mixing (Zeebe and Wolf-Gladrow 2001). In the present study, we quantify the effect of the NEM on the CO_2 balance, which is almost exclusively controlled by aerobic degradation rates because the contributions of denitrification and NPP to the net ecosystem balance are small. Nitrification, a process triggered by the transport and/or production of NH_4 in oxygenated waters, favors outgassing through its effect on pH, which shifts the acid-base equilibrium of carbonate species and increases the CO_2 concentration. The contribution of supersaturated riverine waters to the overall estuarine CO_2 dynamics is calculated as difference between all the other processes creating or consuming CO_2. Figure 10a presents the contribution of the annually integrated *NEM*, nitrification and evasion of supersaturated, DIC enriched riverine waters to the total outgassing for each system, as well as for individual regions of the domain. The calculation of these annual values is based on the sum of the seasonal fluxes. Model results reveal that, regionally, the *NEM* supports about 50% of the estuarine CO_2 outgassing, while nitrification and riverine DIC inputs sustain about 17% and 33% of the CO_2 emissions, respectively. The relative significance of the three processes described above shows important spatial variability. In the NAR, oversaturated riverine waters and NEM respectively sustain 50% and 44% of the outgassing within

Formatted: Font: Not Bold, Not Italic, No underline

Deleted: T

Formatted: Font: Not Bold, Not Italic, No underline

Formatted: Font: Not Bold, Not Italic, No underline

Deleted: (see Regnier et al., 2013b)

Deleted: .

Deleted: 8a

Formatted: Font: Not Bold, Not Italic, No underline

Deleted: Nitrification, a process triggered by the transport and/or production of NH_4 in oxygenated waters, favors outgassing through its effect on pH, which shifts the acid-base equilibrium of carbonate species and increases the CO_2 concentration. In addition, the *NEM* is almost exclusively controlled by aerobic degradation rates because the contribution of denitrification and NPP to the net ecosystem balance is small. ¶

715 the sub-region, while nitrification is of minor importance (6%). In the MAR, the contribution of
716 riverine DIC inputs is significantly lower (~30%) and the main contribution to the outgassing is *NEM*
717 (~50%); nitrification accounting for slightly less than 20% of the outgassing. In the SAR, the riverine
718 contribution is even lower (~20%), and the outgassing is mainly attributed to the *NEM* (~55%) and
719 nitrification (~25%). Therefore, although the model results reveal significant variability across
720 individual systems, a clear latitudinal trend in the contribution to the total FCO_2 emerge from the
721 analysis; the importance of oversaturated riverine water decreasing from North to South, while *NEM*
722 and nitrification increase along the same latitudinal gradient. The increasing relative importance of
723 estuarine biogeochemical processes over riverine DIC inputs as drivers of FCO_2 along the North-
724 South gradient is largely driven by increasing temperatures from North to South, especially in the
725 SAR region (Tab. SI 1).

726 Contrasting patterns across the 3 regions can also be observed with respect to carbon filtering
727 capacities, *CFilt* (Fig. 10b). In the NAR, over 90% of the riverine carbon flux is exported to the coastal
728 ocean. However, in the MAR, the high efficiency of the largest systems in processing organic carbon
729 results in a regional *CFilt* that exceeds 50%. This contrast between the NAR and the MAR and its
730 potential implication for the carbon dynamics of the adjacent continental shelf waters has already
731 been discussed by Laruelle et al. (2015). In the NAR, short estuarine residence results in a much
732 lower removal of riverine carbon by degassing compared to the MAR. Laruelle et al. (2015)
733 suggested that this process could contribute to the weaker continental shelf carbon sink adjacent to
734 the NAR, compared to the MAR. In the SAR, most estuaries remove between 40% and 65% of the
735 carbon inputs. The high temperatures observed and resulting accelerated biogeochemical process
736 rates in this region favor the degradation of organic matter and contribute to increase the estuarine
737 filtering capacity for carbon. However, in the SAR, a large fraction of the OC loads is derived from
738 adjacent salt marshes located along the estuarine salinity gradients, thereby reducing the overall
739 residence time of OC within the systems. The filtering capacity of the riverine OC alone, which
740 transits through the entire estuary, would thus be higher than the one calculated here. As a

Deleted: Table

Deleted: 8b

consequence, highest C retention rates are expected in warm tidal estuaries devoid of salt marshes or mangroves (Cai, 2011).

3.2 Seasonal variability of estuarine carbon dynamics

Carbon dynamics in estuaries of the US East coast not only show a marked spatial variability, but also vary on the seasonal timescale. Table 5 presents the seasonal distribution of *NEM* and FCO_2 for each sub-region. In the NAR, a strong seasonality is simulated for the *NEM* and the summer period contributes more than a third to the annually integrated value. The outgassing reveals a lower seasonal variability and is only slightly higher than summer outgassing during fall and lower during spring. In the MAR, summer contributes more to the *NEM* (>28% of the yearly total) than any other season, but seasonality is less pronounced than in the NAR. Here, FCO_2 is largest in winter and particularly low during summer. In the SAR, summer accounts for 30 % of the NEM, while spring contributes 21 %. FCO_2 is relatively constant throughout the year suggesting that seasonal variations in carbon processing decrease towards the lower latitudes in the SAR. This is partly related to the low variability in river discharge throughout the year in lower latitudes (Tab. SI1). In riverine dominated systems with low residence times, such as, for instance, the Altamaha River estuary, the CO_2 exchange at the air-water interface is mainly controlled by the river discharge because the time required to degrade the entire riverine organic matter flux exceeds the transit time of OC through the estuary. Therefore, the riverine sustained outgassing is highest during the spring peak discharge periods. In contrast, the seasonal variability in FCO_2 in long-residence, marine-dominated systems with large marsh areas (e.g. Sapelo and Doboy Sound) is essentially controlled by seasonal temperature variations. Its maximum is reached during summer when marsh plants are dying and decomposing, as opposed to spring when marshes are in their productive stage (Jiang et al., 2008). These contrasting seasonal trends have already been reported for different estuarine systems in Georgia, such as the Altamaha Sound, the Sapelo Sound and the Doboy Sound (Cai, 2011). At the scale of the entire East coast of the US, the seasonal trends in *NEM* reveal a clear maximum in summer and minimal values during autumn and winter. The seasonality of FCO_2 is much less

Deleted: Table

pronounced because the outgassing of oversaturated riverine waters throughout the year contributes to a large fraction of the FCO_2 and dampens the effect of the temperature dependent processes (*NEM* and denitrification). In our simulations, the competition between temperature and river discharge is the main driver of the seasonal estuarine carbon dynamics is. When discharge increases, the carbon loads increase proportionally and the residence time within the system decreases, consequently limiting an efficient degradation of organic carbon input fluxes. In warm regions like the SAR, the temperature is sufficiently high all year round to sustain high C processing rates and this explains the reduced seasonal variability in NEM.

3.3 Regional carbon budget: a comparative analysis

The annual carbon budget for the entire East coast of the US is summarized in Fig. 11a. The total carbon input to estuaries along the East coast of the US is 4.6 Tg C y^{-1}, of which 42% arrives in organic form and 58% in inorganic form**.** Of this total input, saltmarshes contribute 0.6 Tg C yr^{-1}, which corresponds to about 14% of the total carbon loads and 32% of the organic loads in the region. The relative contribution of the saltmarshes to the total carbon input increases towards low latitudes and is as high as 60% in the SAR region. Model results suggest that 2.7 Tg C y^{-1} is exported to the continental shelf (25% as TOC and 75% as DIC), while 1.9 Tg C y^{-1} is emitted to the atmosphere. The overall carbon filtering capacity of the region thus equals 41% of the total carbon entering the 43 estuarine systems (river + saltmarshes). Because of the current lack of a benthic module in C-GEM, the water column carbon removal occurs entirely in the form of CO_2 outgassing and does not account for the potential contribution of carbon burial in sediments. The estimated estuarine carbon retention presented here is thus likely a lower bound estimate. Reported to the modeled surface area of the region, the total FCO_2 of 1.9 Tg C y^{-1} translates into a mean air water CO_2 flux of about 14 mol C m^{-2} y^{-1}. This value is slightly higher than the estimate of 10.8 mol C m^{-2} y^{-1} calculated by Laruelle et al., (2013) on the basis of local $\overline{FCO_2}$ estimates assumed to be representative of yearly averaged conditions (see section 2.1). The latter was calculated as the

Deleted: fig

Deleted: 9a

Deleted: 47

799 average of 13 annual $\overline{FCO_2}$ values reported in the literature (Tab. 2), irrespective of the size of the
800 systems. This approach is useful and widely used to derive regional and global carbon budgets
801 (Borges et al., 2005; Laruelle et al., 2010; Chen et al., 2013). However, it may lead to potentially
802 significant errors (Volta et al., 2016a) due to the uncertainty introduced by the spatial interpolation
803 of local measurements to large regional surface areas, while useful and widely used to derive
804 regional and global carbon budgets.

805 Regional C budgets are sparse. To our knowledge, the only other published regional assessment of
806 the estuarine carbon and CO_2 dynamics comes from a relatively well studied region: the estuaries
807 flowing into the North Sea in Western Europe (Fig. 11b). This budget was calculated using a similar
808 approach (Volta 2016a) and thus provides an ideal opportunity for a comparative assessment of C
809 cycling in these regions. However, it is important to note that there are also important differences in
810 the applied model approaches and those differences should be taken into account when comparing
811 the derived budgets. In particular, the NW European study is based on a simulation of the 6 largest
812 systems only (Elbe, Scheldt, Thames, Ems, Humber and Weser), accounting for about 40% for the
813 riverine carbon loads of the region. It assumes that the intensity of carbon processing and evasion in
814 all other smaller estuaries discharging into the North Sea (16 % of the carbon loads) can be
815 represented by the average of the 6 largest system simulation results. In addition, the Rhine-Meuse
816 system, which alone accounts for 44% of the carbon riverine inputs of the region, was treated as a
817 passive conduit with respect to carbon due to its very short freshwater residence time (Abril et al.,
818 2002). The contribution of saltmarshes to the regional carbon budget was also ignored because their
819 total surface area is much smaller than along the US East coast (Regnier et al., 2013b). Another
820 important difference is the inclusion of seasonality in the present study while the budget calculated
821 for the North Sea is derived from yearly average conditions (Volta et al., 2016a).

822 Overall, although both regions receive similar amounts of C from rivers (4.6 Tg C y^{-1} and 5.9 Tg C y^{-1}
823 for the East coast of the US and the North Sea, respectively), they reveal significantly different C

Deleted: table
Deleted: 3
Deleted: 9b

filtering capacities. While the estuaries of the East coast of the US filter 41% of the riverine TC loads, those from the North Sea only remove 8% of the terrestrial-derived material. This is partly due to the large amounts of carbon transiting through the 'passive' Rhine-Meuse system. The regional filtering capacity is higher (15%) when this system is excluded from the analysis. However, even when neglecting this system, significant differences in filtering efficiencies between both regions remain. FCO_2 from the North Sea estuaries (0.5 Tg C y^{-1}) is significantly lower than the 1.9 Tg C y^{-1} computed for the East coast of the US. The reason for the lower evasion rate in NW European estuaries is essentially twofold. First, the total cumulative surface area available for gas exchange is significantly lower along the North Sea, in spite of comparable flux densities calculated using the entire estuarine surface areas of both regions (14 mol C m^{-2} y^{-1} and 23 mol C m^{-2} y^{-1} for the East coast of the US and the North Sea, respectively). Second, although the overall riverine carbon loads are comparable in both regions (Fig. 11), the ratio of organic to inorganic matter input is much lower in the North Sea area because of the regional lithology is dominated by carbonate rocks and mixed sediments that contain carbonates (Dürr et al., 2005; Hartmann et al., 2012). As a consequence, TOC represents less than 20% of the riverine loads and only 10% of the carbon exported to the North Sea. In both regions, however, the increase of the inorganic to organic carbon ratio between input and output is sustained by a negative NEM (Fig. 11). Although the ratios themselves may significantly vary from a region of the world to the other as evidenced by these two studies, a NEM driven increase of the inorganic fraction within carbon load along the estuarine axis is consistent with the global estuarine carbon budget proposed by Bauer et al. (2013). In the East coast of the US, the respiration of riverine OC within the estuarine filter is partly compensated by OC inputs from marshes and mangroves in such a way that the input and export IC/OC ratios are closer than in the North Sea region.

Deleted: 9

Deleted: 9

3.4 Scope of applicability and model limitations

Complex multidimensional models are now increasingly applied to quantitatively explore carbon and nutrient dynamics along the land-ocean transition zone over seasonal and even annual timescales

(Garnier et al., 2001; Arndt et al., 2007, 2009; Arndt and Regnier, 2007; Mateus et al., 2012). However, the application of such complex models remains limited to individual, well-constrained systems due their high data requirements and computational demand resulting from the need to resolve important physical, biogeochemical and geological processes on relevant temporal and spatial scales. The one-dimensional, computationally efficient model C-GEM has been specifically designed to reduce data requirements and computational demand and to enable regional/global scale applications (Volta et al., 2014, 2016a). However, such a low data demand and computational efficiency inevitably requires simplification. The following paragraphs critically discus these simplifications and their implications.

Spatial resolution

Here, C-GEM is used with a 0.5° spatial resolution. While this resolution captures the features of large systems, it is still very coarse for relatively small watershed, such as those of the St. Francis River, Piscataqua River, May River or the Sapelo River. For instance, the 5 estuaries reported by Hunt et al. (2010, 2011, see section 2.6) are all small systems contained by the same watershed at a 0.5° resolution. Only watersheds whose area spans several grid cells can be properly identified and represented (i.e. Merrimack or Penobscot with 6 and 9 cells, respectively).

Hydrodynamic and Transport Model

C-GEM is based on a theoretical framework that uses idealized geometries and significantly reduces data requirements. These idealized geometries are fully described by three, easily obtainable geometrical parameters (B, b_0, H). The model thus approximates the variability of estuarine width and cross-section along the longitudinal axis through a set of exponential functions. A comprehensive sensitivity study (Volta et al., 2014) has shown that integrated process rates are generally sensitive to changes in these geometrical parameters because of their control on estuarine residence times. For instance, Volta et al. (2014) demonstrated that the NEM, is particularly sensitive

to the convergence length. Similarly, the use of constant depth profile may lead to variations of about 10% in NEM (Volta et al., 2014). Nevertheless, geometrical parameters are generally easy to constrain, especially well-monitored regions such as the US east coast. Here, all geometrical parameters are constrained on the basis of observed estuarine surface areas and average water depths. In addition, the model also accounts for the slope of the estuarine channel. This approach ensures that simulated estuarine surface areas, volumes and, thus, residence times are in good agreement with those of the real systems and minimizes uncertainties associated to the physical set-up.

In addition, the one-dimensional representation of the idealized estuarine systems does not resolve two- or three-dimensional circulation features induced by complex topography and density driven circulation. While C-GEM performs well in representing the dominant longitudional gradients, its applicability to branched systems or those with aspect ratios for which a dominant axis is difficult to identify (e.g. Blackwater estuary, UK; Pearl River estuary, China; Tagus estuary, Portugal; Bay of Brest, France) is limited.

Biogeochemical Model

Although the reaction network of C-GEM accounts for all processes that control estuarine FCO_2 (Borges and Abril, 2012; Cai, 2011), several, potentially important processes, such as benthic-pelagic exchange processes, phosphorous sorption/desorption and mineral precipitation, a more complex representation of the local phytoplankton community, grazing by higher trophic levels, or multiple reactive organic carbon pools are not included. Although these processes are difficult to constrain and their importance for FCO_2 is uncertain, the lack of their explicit representations induces uncertainties in Cfilt. In particular, the exclusion of benthic processes such as organic matter degradation and burial in estuarine sediments could result in an underestimation of Cfilt. However, because very little is known on the long term fate of organic carbon in estuarine sediments, setting up and calibrating a benthic module proves a difficult task. Furthermore, to a certain degree model

parameters (such as organic matter degradation and denitrification rate constant) implicitly account for benthic dynamics. We nonetheless acknowledge that, by ignoring benthic processes and burial in particular, our estimates for the estuarine carbon filtering may be underestimated, particularly in the shallow systems of the SAR.

Biogeochemical model parameters for regional and global applications are notoriously difficult to constrain (Volta et al., 2016b). Model parameters implicitly account for processes that are not explicitly resolved and their transferability between systems is thus limited. In addition, published parameter values are generally biased towards temperate regions in industrialized countries (Volta et al., 2016b). A first order estimation of the parameter uncertainty associated to the estuarine carbon removal efficiency (CFilt) can be extrapolated from the extensive parameter sensitivity analyses carried out by Volta et al. (2014, 2016b). These comprehensive sensitivity studies on end-member systems have shown that the relative variation in Cfilt when a number of key biogeochemical parameters are varied by two orders of magnitude varies by is ±15 % in prismatic (short residence time on order of days) to ±25 % in funnel-shaped (long residence time) systems. Thus, assuming that uncertainty increases linearly between those bounds as a function of residence time, an uncertainty estimate can be obtained for each of our modelled estuary. With this simple method, the simulated regional Cfilt of 1.9 Tg C yr-1 would be associated with an uncertainty range comprised between 1.5 and 2.2 Tg C yr^{-1}. Our regional estuarine CO_2 evasion estimate is thus reported with moderate confidence. Furthermore, in the future, this uncertainty range could be further constrained using statistical methods such as Monte Carlo simulations (e.g. Lauerwald et al., 2015).

Boundary Conditions and Forcings

In addition, simulations are only performed for climatological means over the period 1990-2010 without resolving interannual and secular variability. Boundary conditions and forcings are critical as they place the modelled system in its environmental context and drive transient dynamics. However,

for regional applications, temporally resolved boundary conditions and forcings are difficult to constrain. C-GEM places the lower boundary condition 20 km from the estuarine mouth into the coastal ocean and the influence of this boundary condition on simulated biogeochemical dynamics is thus limited. At the lower boundary condition, direct observations for nutrients and oxygen are extracted from databases such as the World Ocean Atlas (Antonov et al., 2014). However, lower boundary conditions for OC and pCO_2 (zero concentration for OC and assumption of pCO_2 equilibrium at the sea side) are simplified. This approach does not allow addressing the additional complexity introduced by biogeochemical dynamics in the estuarine plume (see Arndt et al., 2011). Yet, these dynamics only play a secondary role in the presented study that focuses on the role of the estuarine transition zone in processing terrestrial-derived carbon.

Constraining upper boundary conditions and forcings is thus more critical. Here, C-GEM is forced by seasonally-averaged conditions for Q, T, and radiation. To date, GlobalNEWS only provide yearly-averaged conditions for a number of upper boundary conditions (Seitzinger et al., 2005; Mayorga et al., 2010), representative of the year 2000. Simulations are thus only partly transient (induced by seasonality in Q, T and radiation) and do not resolve short-lived events such as storms or extreme drought conditions. In addition, direct observations of upper boundary conditions are rarely available- in particular over seasonal or annual timescales. For the US East Coast estuaries, direct observations are only available for O_2, chlorophyll a, DIC and Alk. For DIC and alkalinity and boundary conditions are constrained by calculating the average concentration over a period of about three decades. In addition, observational data is extracted at the station closest to the model's upper boundary, which might be still located several kilometres upstream or downstream of the model boundary. Upper boundary conditions of POC, DOC, DIN, DIP, DSi are extracted from GlobalNews and thus model-derived. As a consequence, our results are thus intimately dependent on the robustness of the GlobalNEWS predictions. These values are usually only considered robust estimates for watersheds larger than ~10 cells (Beusen et al., 2005), which only correspond to 13 of the 43 estuaries modelled in this study.

Model-data comparison

The generic nature of the applied model approach and, in particular the application of seasonally/annually averaged or model-deduced boundary conditions renders a direct validation of model results on the basis of local and instantaneous observational data (e.g. longitudinal profiles), which is likely not representative of these long-term average conditions, difficult. Therefore, model performance is evaluated on the basis of spatially aggregated estimates (e.g. regional FCO_2 estimates based on local measurements) rather than system-to-system comparisons with longitudinal profile from specific days. However, note that the performance of C-GEM has been intensively tested by specific model-data comparisons for a number of different systems (e.g. Volta et al., 2014, 2016a) and we are thus confident of its predictive capabilities.

Despite the numerous simplifying assumptions inevitably required for such a regional assessment of carbon fluxes along the land-ocean continuum, the presented approach does nevertheless provide an important step forward in evaluating the role of land-ocean transition systems in the global carbon cycle. It provides a first robust estimate of carbon dynamics based on a theoretically well-founded and carefully tested, spatially and temporally resolved model approach. This approach provides novel insights that go beyond those gained through traditionally applied zero-salinity method or box model approaches. In addition, it also highlights critical variables and data gaps and thus helps guide efficient monitoring strategies.

3.5 Towards predictors of the estuarine carbon processing

Deleted: 4

The mutual dependence between geometry and transport in tidal estuaries and, ultimately, their biogeochemical functioning (Savenije, 1992; Volta et al., 2014) allows relating easily extractable parameters linked to their shape or their hydraulic properties to biogeochemical indicators. In this section, we explore the relationships between such simple physical parameters and indicators of the estuarine carbon processing $\overline{NEM}$, $\overline{FCO_2}$ and *CFilt*. In order to account for the effect of temperature

on C dynamics, -$\overline{NEM}$ and $\overline{FCO_2}$ are also normalized to the same temperature (arbitrarily chosen to be 0 degree). These normalized values are obtained by dividing -$\overline{NEM}$ and $\overline{FCO_2}$ by a Q_{10} function *f(T)* (see Volta et al., 2014). This procedure allows accounting for the exponential increase in the rate of several temperature dependent processes contributing to the NEM (i.e. photosynthesis, organic carbon degradation…). Applying the same normalization to -$\overline{NEM}$ and $\overline{FCO_2}$ is a way of testing how intimately linked *NEM* and FCO_2 are in estuarine systems. Indeed linear relationships relating one to the other have been reported (Mayer and Eyre, 2012). The three indicators are then investigated as a function of the ratio between the estuarine surface *S* and the seasonal river discharge *Q*. The surface area is calculated from the estuarine width and length, as described by equation 2, in order to use a parameter which is potentially applicable to other regions for which direct estimates of the real estuarine surface area is not available. Since the fresh water residence time of a system is obtained by dividing volume by river discharge, the S/Q ratio is also intimately linked to residence time. Here, we choose to exclude the estuarine depth from the analysis because this variable cannot be easily quantified from maps or remote sensing images and would thus compromise the applicability of a predictive relationship on the global scale. However, from dimensional analysis, S/Q can be viewed as a water residence time normalized to meter depth of water. As shown by equation 3, *S* only requires constraining *B0* and width convergence length *b*, two parameters that can readily be extracted from the Google Earth engine. Global database of river discharges, as for instance RivDIS (Vörösmarty et al., 1996) are also available in such a way that the S/Q ratio can potentially be extracted for all estuaries around the globe.

Figure 12a reveals that small values of S/Q are associated with the most negative $\overline{NEM}$ / $f(T)$. The magnitude of the $\overline{NEM}$ then exponentially decreases with increasing values of S/Q. Estuaries characterized by small values of *S/Q* are mainly located in the NAR sub-region and correspond to small surface area, and thus short residence time systems. It is possible to quantitatively relate -$\overline{NEM}$ /$f(T)$ and S/Q through a power law function (y = 25.85 $x^{-0.64}$ with a r^2 = 0.82). The coefficient

Deleted:

Formatted: Font: Italic

Formatted: Font: Italic

Formatted: Font: Italic, Subscript

Deleted: 10a

of determination remains the same when excluding estuaries from the NAR region and the equation itself is not significantly different, although those estuaries on their own do not display any statistically significant trend (Tab. 6). The decrease in the intensity of the net ecosystem metabolism in larger estuaries (Fig 8), characterized by high S/Q ratios, can be related to the extensive consumption of the organic matter pool during its transit through the estuarine filter. However, when reported to the entire surface area of the estuary, larger systems (with high values of S/Q) still reveal the most negative surface integrated *NEM* (Fig. 12b). It can also be noted that some estuaries from the NAR region display very low values of *–NEM*. These data points correspond to fall and winter simulations for which the temperature was relatively cold (<5 °C) and biogeochemical processing was very low.

The overall response of $\overline{FCO_2}/f(T)$ to S/Q is comparable to that of -$\overline{NEM}/f(T)$ (Fig. 12c), with lower values of $\overline{FCO_2}$ observed for high values of S/Q. However, for S/Q < 3 days m^{-1}, the $\overline{FCO_2}$ values are very heterogeneous and contain many, low $\overline{FCO_2}$ outliers from the NAR region. These data points generally correspond to low water temperature conditions which keep pCO_2 low, even if the system generates enough CO_2 internally via NEM. Thus, the well-documented correlation between $\overline{NEM}$ and $\overline{FCO_2}$ (Maher and Eyre, 2012) does not seem to hold for systems with very short residence times. For systems with S/Q > 3 days m^{-1}, we obtain a regression FCO_2 = -0.64 x *NEM* + 5.96 with a r^2 of 0.46, which compares well with the relation FCO_2 = -0.42 x *NEM* + 12 proposed by Maher and Eyre (2012) who used 24 seasonal estimates from small Australian estuaries. However, our results suggest that this relationship cannot be extrapolated to small systems such as those located in the NAR. Figure 12d, which reports non-normalized FCO_2 reveals a monotonous increase of FCO_2 with S/Q. This suggests that, unlike the *NEM* for which the normalization by a temperature function allowed explaining most of the variability; FCO_2 is mostly controlled by the water residence time within the system. Discharge is the main FCO_2 driver in riverine dominated systems, while interactions with marshes are driving the outgassing in marine dominated systems surrounded by

Deleted: table

Deleted: 6

Deleted: fig

Deleted: 10b

Deleted: 10c

Deleted: m

Formatted: Font: Italic

marshes. Net aquatic biological production (NEM being negative or near 0) in large estuaries (with large S/Q) is another important reason for low FCO_2 in such systems. For example, despite the higher CO_2 degassing flux in the upper estuary of the Delaware, strong biological CO_2 uptake in the mid-bay and near zero NEM in the lower bay result in a much lower FCO_2 for the entire estuary (Joesoef et al. 2015). In systems with S/Q < 3 days m^{-1}, the short residence time prevents the excess CO_2 of oversaturated water from being entirely exchanged with the atmosphere and simulations reveal that the estuarine waters are still oversaturated in CO_2 at the estuarine mouth. Thus, the inorganic carbon, produced by the decomposition of organic matter, is not outgassed within the estuary but exported to the adjacent continental shelf waters. This result is consistent with the observation-based hypothesis of Laruelle et al. (2015) for the NAR estuaries. As a consequence of the distinct behavior of short residence time systems, the coefficient of determination of the best-fitted power law function relating $\overline{FCO_2}$ and S/Q is only significant if NAR systems are excluded ($y = 31.64\ x^{-0.58}$ with a $r^2 = 0.70$). This thus suggest that such relationships (as well as that proposed by Maher and Eyre, 2012) cannot be applied to any system but only those for which S/Q>3 day m^{-1}.

Finally, Fig. 12e reports the simulated mean seasonal carbon filtering capacities as a function of the depth normalized residence time. Not surprisingly, and in overall agreement with previous studies on nutrient dynamics in estuaries (Nixon et al., 1996), the carbon filtering capacity increases with S/Q. The best statistical relation between *CFilt* and S/Q is obtained when including all 3 regions, resulting in $r^2 = 0.70$ ($y = 40.64 \log_{10}(x) + 11.84$). Very little C removal occurs in systems with S/Q < 1 day m^{-1}. For systems characterized by longer depth-normalized residence times, *CFilt* increases regularly, and reaches 100% for S/Q > 100 day m^{-1}. Such high values are only observed for very large estuaries from the MAR region (Delaware and Chesapeake Bays); the majority of our systems had an *S/Q* range between 1 and 100 day m^{-1}. The quantitative assessment of estuarine filtering capacities is further complicated by the complex interplay of estuarine and coastal processes. Episodically, marked spatial variability in concentration gradients near the estuarine mouth may lead to a reversal of net material fluxes from coastal waters into the estuary (Regnier at al., 1998; Arndt et al. 2011).

Formatted: Superscript

Deleted: Figure

Deleted: 10e

Our results show that this feature is particularly significant for estuaries with a large width at the mouth and short convergence length (funnel shaped or 'Bay type' systems). These coastal nutrient and carbon inputs influence the internal estuarine C dynamics and lead to filtering capacities that can exceed 100%. This feature is particularly significant in summer, when riverine inputs are low and the marine material is intensively processed inside the estuary.

Previous work investigated the relationship between fresh water residence time and nutrient retention (Nixon et al., 1996; Arndt et al., 2011; Laruelle, 2009). These studies, however, were constrained by the scarcity of data. For instance, the pioneering work of Nixon et al. (1996) only relied on a very limited number (<10) of quite heterogeneous coastal systems, all located along the North Atlantic. Here, our modeling approach allows us to generate 172 (43 x 4) data points, each representing a system-scale biogeochemical behavior. Together, this database spans the entire spectrum of estuarine settings and climatic conditions found along the East coast of the US. In addition, the ratio S/Q used as master variable for predicting temperature normalized -$\overline{NEM}$, $\overline{FCO_2}$ and *CFilt* only requires a few easily accessible geometric parameters (B0, b and L) and an estimate of the river discharge. While it is difficult to accurately predict $\overline{FCO_2}$ for small systems such as those located in the NAR region, the relationships found are quite robust for systems in which S/Q > 3 days m^{-1}. Most interestingly, *CFilt* values reveal a significant correlation with S/Q and could be used in combination with global riverine carbon delivery estimates such as GlobalNews 2 (Mayorga et al., 2010) to constrain the estuarine CO_2 evasion and the carbon export to the coastal ocean at the continental and global scales.

4. Conclusions

This study presents the first complete estuarine carbon budget for the East coast of the US using a modeling approach. The structure of the model C-GEM relies on a restricted number of readily available global datasets to constrain boundary conditions and limits the number of geometrical and physical parameters to be constrained. Our simulations predict a total CO_2 outgassing of 1.9 Tg C y^{-1}

for all tidal estuaries of the East coast of the US. This quantification accounts for the seasonality in estuarine carbon processing as well as for distinct individual behaviors among estuarine types (marine or river dominated). The total carbon output to the coastal ocean is estimated at 2.7 TgC y^{-1}, and the carbon filtering capacity with respect to riverine, marshes and mangrove inputs is thus on the order of 40%. This value is significantly higher than the recently estimated C filtering capacity for estuaries surrounding the North Sea using a similar approach (Volta et al., 2016a), mainly because the surface area available for gas exchange and the draining lithology limits the CO_2 evasion in the NW European systems. At the regional scale of the US East coast estuaries, net heterotrophy is the main driver (50%) of the CO_2 outgassing, followed by the ventilation of riverine supersaturated waters entering the estuarine systems (32%) and nitrification (18%). The dominant mechanisms for the gas exchange and the resulting carbon filtering capacities nevertheless reveal a clear latitudinal pattern, which reflects the shapes of estuarine systems, climatic conditions and dominant land-use characteristics.

Our model results are used to derive predictive relationships relating the intensity of the area-based Net Ecosystem Metabolism ($\overline{NEM}$), air-water CO_2 exchange ($\overline{FCO_2}$) and the carbon filtering capacity (*CFilt*) to the depth normalized residence time, expressed as the ratio of the estuarine surface area to the river discharge. In the future, such simple relationships relying on readily available geometric and hydraulic parameters could be used to quantify carbon processing in areas of the world devoid of direct measurements. However, it is important to note that such simple relationships are only valid over the range of boundary conditions and forcings explored and may not be applicable to conditions that fall outside of this range. In regions with better data coverage, such as the one investigated here, our study highlights that the regional-scale quantification, attribution, and projection of estuarine biogeochemical cycling are now at reach.

Formatted: Font: Not Bold, Not Italic, No underline

Deleted: prediction

5. Acknowledgements

G. G. Laruelle is Chargé de recherches du F.R.S.-FNRS at the Université Libre de Bruxelles. The research leading to these results has received funding from the European Union's Horizon 2020 research and innovation programme under the Marie Sklodowska-Curie grant agreement No 643052 (C-CASCADES project). The authors thank V. L. Mulder for her thorough reading of the manuscript upon submission.

References:

Abril, G., Nogueira, M., Etcheber, H., Cabeçadas, G., Lemaire, E., and Brogueira, M.J.: Behaviour of organic carbon in nine contrasting European estuaries. Estuar. Coast. Shelf Sci., 54, 241-262, 2002.

Antonov, J.I., Seidov, D., Boyer, T.P., Locarnini, R.A., Mishonov, A.V., Garcia, H.E., Baranova, O.K., Zweng, M.M., and Johnson, D.R.: World Ocean Atlas 2009, Volume 2: Salinity. S., 2010.

Arndt, S., Vanderborght, J.P., and Regnier, P.: Diatom growth response to physical forcing in a macrotidal estuary: Coupling hydrodynamics, sediment transport, and biogeochemistry. Journal of Geophysical Research C: Oceans, 112(5), 2007.

Arndt, S. and Regnier, P.: A model for the benthic-pelagic coupling of silica in estuarine ecosystems: sensitivity analysis and system scale simulation, Biogeosciences, 4, 331–352, doi:10.5194/bg-4-331-2007, 2007.

Arndt, S., Regnier, P., and Vanderborght, J.P.: Seasonally-resolved nutrient export fluxes and filtering capacities in a macrotidal estuary. Journal of Marine Systems, 78(1), 42-58, 2009.

Arndt, S., Lacroix, G., Gypens, N., Regnier, P., and Lancelot, C.: Nutrient dynamics and phytoplankton development along an estuary-coastal zone continuum: A model study. Journal of Marine Systems, 84(3-4), 49-66, 2011.

Atlas, R., Hoffman, R.N., Ardizzone, J., Leidner, S.M., Jusem, J.C., Smith, D.K. and Gombos, D.: A cross-calibrated, multiplatform ocean surface wind velocity product for meteorological and oceanographic applications. Bulletin of the American Meteorological Society, 92(2), 157-174, 2011.

Bauer, J.E., Cai, W.J., Raymond, P.A., Bianchi, T.S., Hopkinson, C.S., and Regnier, P.A.G.: The changing carbon cycle of the coastal ocean. Nature, 504(7478), 61-70, 2013.

Beusen, A. H.W., Dekkers, A. L. M., Bouwman, A. F., Ludwig,W., and Harrison, J.: Estimation of global river transport of sediments and associated particulate C, N, and P, Global Biogeochem. Cy., 19, GB4S05, doi:10.1029/2005GB002453, 2005.

Beusen, A.H.W., Bouwman, A.F., Dürr, H.H., Dekkers, A.L.M., and Hartmann, J.: Global patterns of dissolved silica export to the coastal zone: Results from a spatially explicit global model. Global Biogeochemical Cycles, 23, GB0A02, doi:10.1029/2008GB003281, 2009.

Billen, G., Thieu, V., Garnier, J., and Silvestre, M.: Modelling the N cascade in regional waters: The case study of the Seine, Somme and Scheldt rivers, Agr. Ecosyst. Environ., 133, 234–246, 2009.

Borges, A.V., Delille, B., and Frankignoulle, M.: Budgeting sinks and sources of CO_2 in the coastal ocean: Diversity of ecosystems counts. Geophys. Res. Lett., 32(14), L14601, 2005.

Borges, A.V., and Abril, G.: Carbon Dioxide and Methane Dynamics in Estuaries. In: E. Wolanski and D.S. McLusky (Editors), Treatise on Estuarine and Coastal Science. Academic Press, Waltham, pp. 119–161, 2012.

Bricker, S., Longstaff, B., Dennison, W., Jones, A., Boicourt, K., Wicks, C., and Woerner, J.: Effects of Nutrient Enrichment In the Nation's Estuaries: A Decade of Change, NOAA, MD, 2007.

Brock, T.D.: Calculating solar radiation for ecological studies. Ecological Modelling, 14(1-2), 1-19, 1981.

Caffrey, J.: Factors controlling net ecosystem metabolism in U.S. estuaries. Estuaries, 27(1), 90-101, 2004.

Cai, W.J., and Wang, Y.: The chemistry, fluxes, and sources of carbon dioxide in the estuarine waters of the Satilla and Altamaha Rivers, Georgia. Limnology and Oceanography, 43(4), 657-668, 1998.

Cai, W.J., Wang, Y., and Hodson, R. E.: Acid-base properties of dissolved organic matter in the estuarine waters of Georgia, USA. Geochimica et Cosmochimica Acta, 62(3), 473-483, 1998.

Cai, W.J., Pomeroy, L.R., Moran, M.A., and Wang, Y.: Oxygen and carbon dioxide mass balance for the estuarine-intertidal marsh complex of five rivers in the southeastern U.S. Limnology and Oceanography, 44, 639-649, 1999.

Deleted: ¶

Formatted: English (U.K.)

Formatted: English (U.K.)

Formatted: English (U.K.)

Cai, W.J.: Estuarine and coastal ocean carbon paradox: CO_2 sinks or sites of terrestrial carbon incineration? Ann. Rev. Mar. Sci., 3, 123-145, 2011.

Chen, C.-T.A., Huang, T.-H., Fu, Y.-H., Bai, Y., and He, X.: Strong sources of CO2 in upper estuaries become sinks of CO2 in large river plumes. Current Opinion in Environmental Sustainability, 4(2), 179-185, 2012.

Chen, C.-T. A., Huang, T.-H., Chen, Y.-C., Bai, Y., He, X., and Kang, Y.: Air-sea exchanges of CO2 in the world's coastal seas, Biogeosciences, 10, 6509–6544, doi:10.5194/bg-10-6509-2013, 2013.

Dai, T., and Wiegert, R.G.: Estimation of the primary productivity of Spartina alterniflora using a canopy model. Ecography, 19(4), 410-423, 1996.

Dufore, C. M.: Spatial and Temporal Variations in the Air-Sea Carbon Dioxide Fluxes of Florida Bay, Gratuate School Thesis, University of South Florida, 2012.

Dürr, H.H., Meybeck, M., and Dürr, S.H.: Lithological composition of the Earth's continental surfaces derived from a new digital map emphasizing riverine material transfer. Glob. Biogeochem. Cycles 19 (4), GB4S10, 2005.

Dürr, H.H., Laruelle, G.G., van Kempen, C.M., Slomp, C.P., Meybeck, M., and Middelkoop, H.: Worldwide Typology of Nearshore Coastal Systems: Defining the Estuarine Filter of River Inputs to the Oceans. Estuaries and Coasts, 34(3), 441-458, 2011.

EPA (2009). "1970 - 2008 Average annual emissions, all criteria pollutants in MS Excel." National Emissions Inventory (NEI) Air Pollutant Emissions Trends Data. Office of Air Quality Planning and Standards. Available online at <http://www.epa.gov/ttn/chief/trends/index.html>

Fekete, B.M., Vörösmarty, C.J., and Grabs, W.: High-resolution fields of global runoff combining observed river discharge and simulated water balances. Global Biogeochemical Cycles, 16(3), 15-1, 2002.

Fischer, H. B.: Mixing and Dispersion in Estuaries, Annu. Rev. Fluid Mech., 8, 107–133, 1976.Friedrichs, M.A.M., and Hofmann, E.E.: Physical control of biological processes in the central equatorial Pacific Ocean. Deep-Sea Research Part I: Oceanographic Research Papers, 48(4), 1023-1069, 2001.

Garcia, H.E., Locarnini, R.A., Boyer, E.W., Antonov, A., Baranova, O.K., Zweng, M.M., and Johnson, D.R.: World Ocean Atlas 2009, Volume 3: Dissolved Oxygen, Apparent Oxygen Utilization, and Oxygen Saturation, 2010a.

Garcia, H.E., Locarnini, R.A., Boyer, E.W., Antonov, J.I., Baranova, O.K., Zweng, M.M., and Johnson, D.R.: World Ocean Atlas 2009, Volume 4: Nutrients (phosphate, nitrate, silicate), 2010b.

Garnier, J., Servais, P., Billen, G., Akopian, M., and Brion, N.: Lower Seine River and Estuary (France) Carbon and Oxygen Budgets During Low Flow, Estuaries, 24, 964–976, 2001.

Harrison, J.A., Caraco, N., and Seitzinger, S.P.: Global patterns and sources of dissolved organic matter export to the coastal zone: Results from a spatially explicit, global model. Global Biogeochemical Cycles, 19(4), GB4S03, doi:10.1029/2004GB002357, 2005.

Hartmann, J., Jansen, N., Dürr, H.H., Kempe, S., and Köhler, P.: Global CO_2 consumption by chemical weathering: What is the contribution of highly active weathering regions? Global Planet. Change, 69(4), 185-194, 2009.

Hartmann, J., Dürr, H.H., Moosdorf, N., Meybeck, M., and Kempe, S.: The geochemical composition of the terrestrial surface (without soils) and comparison with the upper continental crust. Int. J. Earth Sci. 101, 365-376, 2012.

Herrmann, M., Najjar, R.G., Kemp, W.M., Alexander, R.B., Boyer, E.W., Cai, W.-J., Griffith, P.C., Kroeger, K.D., McCallister, S.L., and Smith, R.A.: Net ecosystem production and organic carbon balance of U.S. East Coast estuaries: A synthesis approach, Global Biogeochem. Cycles, 29, doi:10.1002/2013GB004736, 2015.

Hofmann, A.F., Soetaert, K., and Middelburg, J.J.: Present nitrogen and carbon dynamics in the Scheldt estuary using a novel 1-D model. Biogeosciences, 5(4), 981-1006, 2008.

Deleted: F

Hofmann, E.E., Cahill, B., Fennel, K., Friedrichs, M.A.M., Hyde, K., Lee, C., Mannino, A., Najjar, R.G., O'Reilly, J.E., Wilkin, J., and Xue, J.: Modeling the dynamics of continental shelf carbon. Ann Rev Mar Sci. 3, 93-122, 2011.

Hunt, C. W., Salisbury, J. E., Vandemark, D., and McGillis, W.: Contrasting Carbon Dioxide Inputs and Exchange in Three Adjacent New England Estuaries. Estuar. Coast., 34, 68–77, doi:10.1007/s12237-010-9299-9, 2010.

Hunt, C.W., Salisbury, J.E., Vandemark, D., and McGillis, W.: Contrasting Carbon Dioxide Inputs and Exchange in Three Adjacent New England Estuaries. Estuaries and Coasts, 34(1), 68-77, 2011.

Ippen, A.T., and Harleman, D.R.F.: One-dimensional Analysis of Salinity Intrusion in Estuaries, Technical Bulletin No. 5, Committee on Tidal Hydraulics, Corps of Engineers, US Army, Vicksburg, 1961.

Jiang, L.Q., Cai, W.J., and Wang, Y.: A comparative study of carbon dioxide degassing in river- and marine-dominated estuaries. Limnology and Oceanography, 53(6), 2603-2615, 2008.

Jiang, L.-Q., Cai, W.-J., Wang, Y., and Bauer, J. E.: Influence of terrestrial inputs on continental shelf carbon dioxide, Biogeosciences, 10, 839–849, doi:10.5194/bg-10-839-2013, 2013.

Joesoef, A., Huang, W.-J., Gao, Y., and Cai, W.-J.: Air–water fluxes and sources of carbon dioxide in the Delaware Estuary: spatial and seasonal variability, Biogeosciences, 12, 6085-6101, doi:10.5194/bg-12-6085-2015, 2015.

Kent, B.H.: Turbulent diffusion in a Sectionally Homogeneous Estuary, Technical Report 16, Chesapeake Bay Institute, John Hopkins, University, Baltimore, 1958.

Key, R.M., Kozyr, A., Sabine, C.L., Lee, K., Wanninkhof, R., Bullister, J.L., Feely, R.A., Millero, F.J., Mordy, C., and Peng, T.H.: A global ocean carbon climatology: Results from Global Data Analysis Project (GLODAP). Global Biogeochemical Cycles, 18(4), 1-23, 2004.

Laruelle, G.G.: Quantifying nutrient cycling and retention in coastal waters at the global scale, Ph D dissertation, Utrecht University, 2009.

Laruelle, G. G., Regnier, P., Ragueneau, O., Kempa, M., Moriceau, B., Ni Longphuirt, S., Leynaert, A., Thouzeau, G., and Chauvaud, L.: Benthic-pelagic coupling and the seasonal silica cycle in the Bay of Brest (France): new insights from a coupled physical-biological model, Mar. Ecol.-Prog. Ser., 385, 15–32, 2009.

Laruelle, G.G., Dürr, H.H., Slomp, C.P., and Borges, A.V.: Evaluation of sinks and sources of CO_2 in the global coastal ocean using a spatially-explicit typology of estuaries and continental shelves. Geophys. Res. Lett., 37(15), L15607, doi:10.1029/2010GL043691, 2010.

Laruelle, G.G., Dürr, H.H., Lauerwald, R., Hartmann, J., Slomp, C.P., Goossens, N., and Regnier, P.A.G.: Global multi-scale segmentation of continental and coastal waters from the watersheds to the continental margins. Hydrol. Earth Syst. Sci., 17(5), 2029-2051, 2013.

Laruelle, G.G., Lauerwald, R., Rotschi, J. Raymond, P.A., and Regnier, P.: Seasonal response of air-water CO2 exchange along the land-ocean aquatic continuum of the northeast North American coast. Biogeosci. 12, 1447-1458, 2015.

Lauerwald, R., Hartmann, J., Moosdorf, N., Kempe, S., and Raymond, P.A.: What controls the spatial patterns of the riverine carbonate system? — A case study for North America. Chemical Geology, 337–338, 114-127, 2013.

Lauerwald, R., Laruelle, G. G., Hartmann, J., Ciais, P., and Regnier, P. A. G.: Spatial patterns in CO2 evasion from the global river network, Global Biogeochem. Cy., 29, 534–554, doi:10.1002/2014GB004941, 2015.

Leonard, B.: Third-Order Upwinding as a Rational Basis for Computational Fluid Dynamics, in: Computational Techniques and Applications: CTAC-83, edited by: Noye J. and Fletcher C. A. J., Elsevier, North-Holland, 1984.

Le Quéré, C., Peters, G. P., Andres, R. J., Andrew, R. M., Boden, T. A., Ciais, P., Friedlingstein, P., Houghton, R. A., Marland, G., Moriarty, R., Sitch, S., Tans, P., Arneth, A., Arvanitis, A., Bakker, D. C. E., Bopp, L., Canadell, J. G., Chini, L. P., Doney, S. C., Harper, A., Harris, I., House, J. I., Jain, A. K., Jones, S. D., Kato, E., Keeling, R. F., Klein Goldewijk, K., Körtzinger, A., Koven, C.,

Lefèvre, N., Maignan, F., Omar, A., Ono, T., Park, G.-H., Pfeil, B., Poulter, B., Raupach, M. R., Regnier, P., Rödenbeck, C., Saito, S., Schwinger, J., Segschneider, J., Stocker, B. D., Takahashi, T., Tilbrook, B., van Heuven, S., Viovy, N., Wanninkhof, R., Wiltshire, A., and Zaehle, S.: Global carbon budget 2013, Earth Syst. Sci. Data, 6, 235-263, doi:10.5194/essd-6-235-2014, 2014.

Le Quéré, C., Moriarty, R., Andrew, R. M., Canadell, J. G., Sitch, S., Korsbakken, J. I., Friedlingstein, P., Peters, G. P., Andres, R. J., Boden, T. A., Houghton, R. A., House, J. I., Keeling, R. F., Tans, P., Arneth, A., Bakker, D. C. E., Barbero, L., Bopp, L., Chang, J., Chevallier, F., Chini, L. P., Ciais, P., Fader, M., Feely, R. A., Gkritzalis, T., Harris, I., Hauck, J., Ilyina, T., Jain, A. K., Kato, E., Kitidis, V., Klein Goldewijk, K., Koven, C., Landschützer, P., Lauvset, S. K., Lefèvre, N., Lenton, A., Lima, I. D., Metzl, N., Millero, F., Munro, D. R., Murata, A., Nabel, J. E. M. S., Nakaoka, S., Nojiri, Y., O'Brien, K., Olsen, A., Ono, T., Pérez, F. F., Pfeil, B., Pierrot, D., Poulter, B., Rehder, G., Rödenbeck, C., Saito, S., Schuster, U., Schwinger, J., Séférian, R., Steinhoff, T., Stocker, B. D., Sutton, A. J., Takahashi, T., Tilbrook, B., van der Laan-Luijkx, I. T., van der Werf, G. R., van Heuven, S., Vandemark, D., Viovy, N., Wiltshire, A., Zaehle, S., and Zeng, N.: Global Carbon Budget 2015, Earth Syst. Sci. Data, 7, 349-396, doi:10.5194/essd-7-349-2015, 2015.

Locarnini, R.A., Mishonov, A.V., Antonov, J.I., Boyer, T.P., Garcia, H.E., Baranova, O.K., Zweng, M.M., and Johnson, D.R.: World Ocean Atlas 2009, Volume 1: Temperature, 2010.

Ludwig, W., Probst, J. L., and Kempe, S.: predicting the oceanic input of organic carbon by continental erosion, Global Bio geochem. Cy., 10, 23–41, 1996.

Maher, D.T., and Eyre, B.D.: Carbon budgets for three autotrophic Australian estuaries: Implications for global estimates of the coastal air-water CO2 flux. Global Biogeochem. Cycles, 26(1), GB1032, 2012.

Mateus, M., Vaz, N., and Neves, R.: A process-oriented model of pelagic biogeochemistry for marine systems. Part II: Application to a mesotidal estuary, J. Mar. Syst., 94, 90–101, 2012.

Mayorga, E., Seitzinger, S.P., Harrison, J.A., Dumont, E., Beusen, A.H.W., Bouwman, A.F., Fekete, B.M., Kroeze, C., and Van Drecht, G.: Global Nutrient Export from WaterSheds 2 (NEWS 2): Model development and implementation. Environmental Modelling and Software, 25(7), 837-853, 2010.

Meybeck, M.: Carbon, nitrogen, and phosphorus transport by world rivers. Am. J. Sci., 282(4), 401-450, 1982.

Meybeck, M., Dürr, H. H., and Vörosmarty, C. J.: Global coastal segmentation and its river catchment contributors: A new look at land-ocean linkage, Global Biogeochem. Cy., 20, GB1S90, doi:10.1029/2005GB002540, 2006.

Middelburg, J.J., Klaver, G., Nieuwenhuize, J., Wielemaker, A., De Haas, W., Vlug, T., and Van Der Nat, J.F.W.A.: Organic matter mineralization in intertidal sediments along an estuarine gradient. Marine Ecology Progress Series, 132(1-3), 157-168, 1996.

NASA/NGA: SRTM Water Body Data Product Specific Guidance, Version 2.0, 2003.

Najjar, R.G., Friedrichs, M., and Cai, W.-J. (Editors): Report of The U.S. East Coast Carbon Cycle Synthesis Workshop, January 19-20, 2012. Ocean Carbon and Biogeochemistry Program and North American Carbon Program, 34 pp, 2012.

Nihoul, J. C. J., and Ronday, F.: Modèles d'estuaires partiellement stratifiés, Projet Mer, Vol. 10, Service de la Programmation Scientifique, Bruxelles, Belgium, 71–98, 1976.

Nixon, S.W., J.W. Ammerman, L.P. Atkinson, V.M. Berounsky, G. Billen, W.C. Boicourt, W.R. Boynton, T.M. Church, D.M. Ditoro, R. Elmgren, J.H. Garber, A.E. Giblin, R.A. Jahnke, N.J. P. Owens, M.E.Q. Pilson, and Seitzinger, S.P.: The fate of nitrogen and phosphorus at the land–sea margin of the North Atlantic Ocean. Biogeochemistry 3, 141–180, 1996.

NOAA: National Estuarine Inventory Data Atlas, Volume 1: Physical and Hydrologic Characteristics, National Oceanic and Atmospheric Administration, MD, 1985.

Odum, H.T.: Primary Production in Flowing Waters. Limnol. Oceanogr., 1, 102-117, 1956..

Paerl, H.W., Valdes, L.M., Peierls, B.L., Adolf, J.E., and Harding Jr, L.W.: Anthropogenic and climatic influences on the eutrophication of large estuarine ecosystems. Limnology and Oceanography, 51(1 II), 448-462, 2006.

Platt, T., Gallegos, C. L., and Harrison, W. G.: Photoinhibition of photosynthesis in natural assemblages of marine phytoplankton. J. Mar. Res., 38, 687-701, 1980.

Preddy, W. S.: The mixing and movement of water in the estuary of the Thames, J. Mar. biol. Ass. UK, 33, 645–662, 1954.

Press, W. H., Teukolosky, S. A., Vetterling, W. T., and Flannery, B.P.: Numerical Recipes in C: The Art of Scientific Programming, 2nd Edn., Cambridge University Press, USA, 1992.

Pritchard, D. W.: The Equations of Mass Continuity and Salt Continuity in Estuaries, J. Marine Res., 15, 33–42, 1958.

Raymond, P.A., Caraco, N.F., and Cole, J.J.: Carbon dioxide concentration and atmospheric flux in the Hudson River. Estuaries, 20(2), 381-390, 1997.

Raymond, P.A., Bauer, J.E., and Cole, J.J.: Atmospheric CO2 evasion, dissolved inorganic carbon production, and net heterotrophy in the York River estuary. Limnology and Oceanography, 45(8), 1707-1717, 2000.

Raymond, P.A., and Hopkinson, C.S.: Ecosystem Modulation of Dissolved Carbon Age in a Temperate Marsh-Dominated Estuary. Ecosystems, 6(7), 694-705, 2003.

Raymond, P.A., Hartmann, J., Lauerwald, R., Sobek, S., McDonald, C., Hoover, M., Butman, D., Striegl, R., Mayorga, E., Humborg, C., Kortelainen, P., Dürr, H., Meybeck, M., Ciais, P., and Guth, P.: Global carbon dioxide emissions from inland waters. Nature, 503(7476), 355-359, 2013.

Regnier, P., Wollast, R., and Steefel, C.I.: Long-term fluxes of reactive species in macrotidal estuaries: Estimates from a fully transient, multicomponent reaction-transport model. Marine Chemistry, 58(1-2), 127-145, 1997.

Regnier, P., Mouchet, A., Wollast, R., and Ronday, F.: A discussion of methods for estimating residual fluxes in strong tidal estuaries, Cont. Shelf Res., 18, 1543–1571, 1998.

Regnier, P., and Steefel, C.I.: A high resolution estimate of the inorganic nitrogen flux from the Scheldt estuary to the coastal North Sea during a nitrogen-limited algal bloom, spring 1995. Geochimica et Cosmochimica Acta, 63(9), 1359-1374, 1999.

Regnier, P., Vanderborght, J. P., Steefel, C. I., and O'Kane, J. P.: Modeling complex multi-component reactive-transport systems: Towards a simulation environment based on the concept of a Knowledge Base, Appl. Math. Model., 26, 913–927, 2002.

Regnier, P., Friedlingstein, P., Ciais, P., Mackenzie, F.T., Gruber, N., Janssens, I.A., Laruelle, G.G., Lauerwald, R., Luyssaert, S., Andersson, A.J., Arndt, S., Arnosti, C., Borges, A.V., Dale, A.W., Gallego-Sala, A., Godderis, Y., Goossens, N., Hartmann, J., Heinze, C., Ilyina, T., Joos, F., LaRowe, D.E., Leifeld, J., Meysman, F.J.R., Munhoven, G., Raymond, P.A., Spahni, R., Suntharalingam, P., and Thullner, M.: Anthropogenic perturbation of the carbon fluxes from land to ocean. Nature Geosci, 6(8), 597-607, 2013a.

Regnier, P., Arndt, S., Goossens, N., Volta, C., Laruelle, G.G., Lauerwald, R., and Hartmann, J.: Modelling Estuarine Biogeochemical Dynamics: From the Local to the Global Scale. Aquatic Geochemistry, 19(5-6), 591-626, 2013b.

Riemann, B., Simonsen, P., and Stensgaard, L.: The carbon and chlorophyll content of phytoplankton from various nutrient regimes. Journal of Plankton Research, 11 (5), 1037-1045, 1989.

Rossow, W.B., and Schiffer, R.A.: Advances in understanding clouds from ISCCP. Bull. Amer. Meteorol. Soc., 80, 2261-2288, doi:10.1175/1520-0477(1999)080<2261:AIUCFI>2.0.CO;2, 1999.

Sarma, V.V.S.S., Viswanadham, R., Rao, G.D., Prasad, V.R., Kumar, B.S.K., Naidu, S.A., Kumar, N.A., Rao, D.B., Sridevi, T., Krishna, M.S., Reddy, N.P.C., Sadhuram, Y., and Murty, T.V.R.: Carbon dioxide emissions from Indian monsoonal estuaries. Geophysical Research Letters, 39(3), L03602, 2012.

Savenije, H.H.G.: A one-dimensional model for salinity intrusion in alluvial estuaries. Journal of Hydrology, 85(1-2), 87-109, 1986.
Savenije, H.H.G.: Lagrangian solution of St. Venant's equations for alluvial estuary. Journal of Hydraulic Engineering, 118(8), 1153-1163, 1992.
Savenije, H. H. G. (Ed.): Salinity and Tides in Alluvial Estuaries, 1st Edn., Elsevier, Amsterdam, 2005.
Savenije, H. H. G. (Ed.): Salinity and Tides in Alluvial Estuaries, 2nd Edn., available at: http://salinityandtides.com (last access: 8 March 2015), 2012.
Seitzinger, S. P., Harrison, J. A., Dumont, E., Beusen, A. H. W., and Bouwman, A. F.: Sources and delivery of carbon, nitrogen, and phosphorus to the coastal zone: An overview of Global Nutrient Export from Watersheds (NEWS) models and their application, *Global Biogeochem. Cycles*, 19, GB4S01, doi:10.1029/2005GB002606, 2005.
Schwarz, G.E., Hoos, A.B., Alexander, R.B., and Smith, R.A.: The SPARROW Surface Water-Quality Model: Theory, Application and User Documentation. U.S. Geological Survey, Techniques and Methods Report, Book 6, Chapter B3, Reston, Virginia, 2006
Sharp, J. H., Yoshiyama, K., Parker, Schwartz, M. C., Curless, S. E., Beauregard, A. Y., Ossolinski, J. E., and Davis, A. R.: A Biogeochemical View of Estuarine Eutrophication: Seasonal and Spatial Trends and Correlations in the Delaware Estuary. Estuaries and Coasts, 32, 1023-1043,. doi:10.1007/s12237-009-9210-8, 2009.
Sharp, J. H.: Estuarine oxygen dynamics: What can we learn about hypoxia from long-time records in the Delaware Estuary? Limnol. Oceanogr., 55(2), 2010, 535–548, 2010.
Shih, J.-S., Alexander, R.B., Smith, R.A., Boyer, E.W., Schwarz, G.E., and Chung, S.: An initial SPARROW model of land use and in-stream controls on total organic carbon in streams of the conterminous United States, U. S. Geological Survey, Reston, Virginia, 2010.
Signorini, S.R., Mannino, A., Najjar Jr, R.G., Friedrichs, M.A.M., Cai, W.J., Salisbury, J., Wang, Z.A., Thomas, H., and Shadwick, E.: Surface ocean pCO2 seasonality and sea-air CO2 flux estimates for the North American east coast. Journal of Geophysical Research C: Oceans, 118(10), 5439-5460, 2013.
Simmons, H. B.: Some effects of inland discharge on estuarine hydraulics, Proc. Am. Soc. Civ. Eng.-ASCE, 81, 792, 1955.
Soetaert, K., and Herman, P.M.J.: Nitrogen dynamics in the Westerschelde estuary (SW Netherlands) estimated by means of the ecosystem model MOSES. Hydrobiologia, 311(1-3), 225-246, 1995.
Stets, E.G., and Strieg, R.G.: Carbon export by rivers draining the conterminous united states. Inland Waters, 2(4), 177-184, 2012.
Stigter, C., and Siemons, J.: Calculation of longitudinal salt distribution in estuaries as function of time, Publication Delft Hydraulics Laboratory, 52, The Netherlands, 1967.
Thieu, V., Mayorga, E., Billen, G., and Garnier, J.: Subregional and downscaled global scenarios of nutrient transfer in river basins: Seine-Somme-Scheldt case study. Global Biogeochemical Cycles, 24(2) , 2010.
Tian, H., Chen, G., Liu, M., Zhang, C., Sun, G., Lu, C., Xu, X., Ren, W., Pan, S., and Chappelka, A.: Model estimates of net primary productivity, evapotranspiration, and water use efficiency in the terrestrial ecosystems of the southern United States during 1895-2007. Forest Ecology and Management, 259(7), 1311-1327, 2010.
Tian, H., Chen, G., Zhang, C., Liu, M., Sun, G., Chappelka, A., Ren, W., Xu, X., Lu, C., Pan, S., Chen, H., Hui, D., McNulty, S., Lockaby, G., and Vance, E.: Century-Scale Responses of Ecosystem Carbon Storage and Flux to Multiple Environmental Changes in the Southern United States. Ecosystems, 15(4), 674-694, 2012.
U. S. Fish and Wildlife Service. 2014. National Wetlands Inventory website. U.S. Department of the Interior, Fish and Wildlife Service, Washington, D.C. http://www.fws.gov/wetlands/, last accessed: February 2015.

Vanderborght, J.P., Wollast, R., Loijens, M., and Regnier, P.: Application of a transport-reaction model to the estimation of biogas fluxes in the Scheldt Estuary. Biogeochemistry, 59(1-2), 207-237, 2002.

Vanderborght, J.P., Folmer, I., Aguilera, D.R., Uhrenholdt, T., and Regnier, P.: Reactive-transport modelling of a river-estuarine-coastal zone system: application to the Scheldt estuary. Mar. Chem. 106, 92-110, 2007.

Van der Burgh, P.: Ontwikkeling van een methode voor het voorspellen van zoutverdelingen in estuaria, kanalen and zeeen, Rijkswaterstaat Rapport, The Netherlands, 1972.

Volta, C., Arndt, S., Savenije, H.H.G., Laruelle, G.G., and Regnier, P.: C-GEM (v 1.0): a new, cost-efficient biogeochemical model for estuaries and its application to a funnel-shaped system. Geosci. Model Dev., 7, 1271-1295, doi:10.5194/gmd-7-1271-2014, 2014.

Volta, C., Laruelle, G. G., and Regnier, P.: Regional carbon and CO_2 budgets of North Sea tidal estuaries, Estuarine, Coastal and Shelf Science, 176, 76-90, 2016a.

Volta, C., Laruelle, G. G., Arndt, S., and Regnier, P.: Linking biogeochemistry to hydro-geometrical variability in tidal estuaries: a generic modeling approach, Hydrol. Earth Syst. Sci., 20, 991-1030, doi:10.5194/hess-20-991-2016, 2016b.

Vörösmarty, C.J., Fekete, B., and Tucker, B.A.: River Discharge Database, Version 1.0 (RivDIS v1.0), Volumes 0 through 6. A contribution to IHP-V Theme 1. Technical Documents in Hydrology Series. UNESCO, Paris, 1996.

Wang, Z.A., and Cai, W.J.: Carbon dioxide degassing and inorganic carbon export from a marsh-dominated estuary (the Duplin River): A marsh CO2 pump. Limnology and Oceanography, 49(2), 341-354, 2004.

Deleted: 6(4), 5645-5709,

Deleted: ¶

Table 1: Estimates of total annual riverine input from watersheds to estuaries (Tg C yr^{-1}). The ranges are based on Stets and Striegl (2012), Global NEWS (Mayorga et al. 2010), Hartmann et al. (2009), SPARROW (Shih et al. 2010) and DLEM (Tian et al. 2010, 2012). Modified from Najjar et al. 2012.

	DIC	DOC	POC	TOTAL
NAR	0.2-0.8	0.3-2.1	0.1-0.2	0.6-3.1
MAR	1.4-1.8	0.5-2.3	0.1-0.3	2.0-4.4
SAR	0.4-1.4	0.9-1.6	0.1-0.2	1.4-3.2
TOTAL	2.0-4.0	1.7-6.0	0.3-0.7	4.0-10.7

Table 2: Published local annually averaged estimates of $\overline{FCO_2}$ in mol C m^{-2} yr^{-1} for estuaries along the East coast of the US.”

Name	Lon	Lat	$\overline{FCO_2}$ Observed.	Modeled	Reference
Altamaha Sound	-81.3	31.3	32.4	72.7	Jiang et al. (2008)
Bellamy	-70.9	43.2	3.6	3.9	Hunt et al. (2010)
Cocheco	-70.9	43.2	3.1	3.9	Hunt et al. (2010)
Doboy Sound	-81.3	31.4	13.9	25.7	Jiang et al. (2008)
Great Bay	-70.9	43.1	3.6	3.9	Hunt et al. (2011)
Little Bay	-70.9	43.1	2.4	3.9	Hunt et al. (2011)
Oyster Bay	-70.9	43.1	4	3.9	Hunt et al. (2011)
Parker River estuary	-70.8	42.8	1.1	3.9	Raymond and Hopkinson (2003)
Sapelo Sound	-81.3	31.6	13.5	20.6	Jiang et al. (2008)
Satilla River	-81.5	31	42.5	25.7	Cai and Wang (1998)
York River	-76.4	37.2	6.2	8.1	Raymond et al. (2000)
Hudson River	-74	40.6	13.5	15.5	Raymond et al. (1997)
Florida Bay	-80.68	24.96	1.4	n.a.	Dufore (2012)

Table 3: State variables and processes explicitly implemented in CGEM.

Deleted: 2

State variables		
Name	**Symbol**	**Unit**
Suspended Particulate Mater	SPM	gL^{-1}
Total Organic Carbon	TOC	µM C
Nitrate	NO_3	µM N
Ammonium	NH_4	µM N
Phosphate	DIP	µM P
Dissolved Oxygen	DO	µM O_2
Phytoplankton	Phy	µM C
Dissolved Silica	dSi	µM Si
Dissolved Inorganic Carbon	DIC	µM C
Biogeochemical reactions		
Name	**Symbol**	**Unit**
Gross primary production	GPP	µM C s^{-1}
Net primary production	NPP	µM C s^{-1}
Phytoplankton mortality	M	µM C s^{-1}
Aerobic degradation	R	µM C s^{-1}
Denitrification	D	µM C s^{-1}
Nitrification	N	µM N s^{-1}
O_2 exchange with the atmosphere	FO_2	µM O_2 s^{-1}
CO_2 exchange with the atmosphere	FCO_2	µM C s^{-1}
SPM erosion	E_{SPM}	gL^{-1} s^{-1}
SPM deposition	D_{SPM}	gL^{-1} s^{-1}

Table 4: Yearly averaged surface area (*S*), fresh water discharge (*Q*), residence time (*Rt*), FCO_2 and *NEM* of all simulated estuaries.

long *degrees*	lat *degrees*	*S* km^2	*Q* $m^3 s^{-1}$	*Rt* *days*	$\overline{FCO_2}$ $mol\ C\ m^{-2}\ yr^{-1}$	$\overline{NEM}$ $mol\ C\ m^{-2}\ yr^{-1}$	FCO_2 $10^6\ mol\ C\ yr^{-1}$	*NEM* $10^6\ mol\ C\ yr^{-1}$
NAR								
-67.25	44.75	7	38.5	15	3.7	-37.4	27	-270
-67.25	45.25	12	73.6	15	6.0	-56.7	71	-666
-67.25	45.25	12	73.6	15	13.8	-56.6	162	-666
-67.75	44.75	3	68.5	4	6.7	-63.5	23	-221
-68.25	44.75	14	69.5	19	4.1	-56.2	58	-791
-68.75	44.75	89	309.9	23	27.4	-58.2	2431	-5163
-69.75	44.25	50	626.6	5	32.3	-74.4	1607	-3703
-70.25	43.75	3	25.8	10	2.1	-21.0	7	-71
-70.75	41.75	288	103.6	958	5.0	-4.0	1428	-1146
-70.75	42.25	63	210.7	40	16.2	-32.9	1025	-2081
-70.75	42.75	17	105.8	3	56.3	-69.0	943	-1155
MAR								
-70.75	43.25	31	29.9	11	21.6	-37.4	662	-1146
-71.25	41.75	257	28.2	808	3.9	-2.5	997	-650
-71.75	41.25	21	112.4	4	35.2	-32.6	726	-672
-72.75	40.75	20	25.4	62	30.7	-21.1	623	-430
-72.75	41.25	10	142.5	2	150.8	-36.9	1578	-386
-72.75	41.75	55	476.6	3	55.9	-45.7	3088	-2523
-73.25	40.75	19	26.8	56	31.4	-28.4	608	-550
-74.25	40.75	1192	608.2	126	15.5	-11.8	18432	-14047
-75.25	38.25	399	80.5	172	13.9	-5.0	5558	-2016
-75.25	38.75	354	31.8	357	7.5	-3.0	2659	-1076
-75.25	39.75	1716	499.0	221	10.0	-7.8	17072	-13439
-75.75	39.25	224	18.3	434	7.5	-2.9	1685	-640
-76.25	39.25	3427	717.1	352	8.1	-5.1	27646	-17352
-76.75	37.25	586	272.3	74	15.0	-10.4	8810	-6084
-76.75	37.75	154	36.3	163	10.7	-6.6	1654	-1023
-76.75	39.25	59	71.2	29	48.6	-34.6	2862	-2038
-77.25	38.25	206	30.2	268	6.1	-3.3	1265	-676
-77.25	38.75	568	259.2	118	16.7	-10.8	9488	-6134
SAR								
-78.25	34.25	48	167.4	7	122.5	-62.4	5916	-3015
-79.25	33.25	47	56.3	42	43.4	-36.5	2056	-1728
-79.25	33.75	45	291.4	8	85.1	-78.7	3843	-3551
-79.75	33.25	25	33.8	15	37.9	-32.8	956	-828
-80.25	32.75	25	31.0	50	48.8	-42.5	1214	-1057
-80.25	33.25	92	75.5	61	62.7	-61.2	5769	-5625
-80.75	32.25	71	21.1	182	12.9	-7.0	918	-501
-80.75	32.75	164	63.1	95	20.6	-11.5	3372	-1879
-81.25	31.75	92	71.7	45	25.7	-20.9	2361	-1926
-81.25	32.25	130	379.8	11	51.7	-39.2	6732	-5097
-81.75	30.75	34	18.7	61	17.5	-14.7	602	-505
-81.75	31.25	130	17.7	294	5.5	-4.0	713	-523
-81.75	31.75	56	350.5	4	72.7	-67.4	4068	-3770

Deleted: **Table 3**: Published local annually averaged estimates of $\overline{FCO_2}$ for estuaries along the East coast of the US. ¶ **Name** ...

Table 5: Seasonal contribution to FCO_2 and *NEM* in each the sub-region. The seasons displaying the highest percentages are indicated in bold. Winter is defined as January, February and March, Spring as April, May and June and so on…

Region	*NEM*	winter	spring	summer	fall	FCO_2	winter	spring	summer	fall
	mol C y^{-1}	%	%	%	%	mol C y^{-1}	%	%	%	%
NAR	-16.3 10^9	14.7	21.2	**37.0**	27.2	7.2 10^9	26.3	18.9	26.5	**28.3**
MAR	-72.2 10^9	21.9	25.9	**28.8**	23.4	108.3 10^9	**29.8**	23.3	20.7	26.2
SAR	-30.5 10^9	24.6	20.9	**30.3**	24.2	39.2 10^9	26	23.4	**27**	23.6

1477 **Table 6:** Regressions and associated coefficient of determination between the depth normalized
1478 residence time (S/Q) and -$\overline{NEM}$ / *f(T)*, $\overline{FCO_2}$ / *f(T)* and *CFilt*.

Region	$-\overline{NEM}/f(T)$	$\overline{FCO_2}/f(T)$	*CFilt*
NAR	$y = 27.84\ x^{-0.17}$ $r^2 = 0.11$	$y = 6.07\ x^{0.00}$ $r^2 = 0.00$	$y = 15.08 \log_{10}(x) + 4.86$ $r^2 = 0.40$
MAR	$y = 26.03\ x^{-0.63}$ $r^2 = 0.86$	$y = 34.36\ x^{-0.58}$ $r^2 = 0.68$	$y = 40.46 \log_{10}(x) + 9.60$ $r^2 = 0.70$
SAR	$y = 28.36\ x^{-0.71}$ $r^2 = 0.76$	$y = 32.82\ x^{-0.66}$ $r^2 = 0.80$	$y = 23.19 \log_{10}(x) + 43.71$ $r^2 = 0.46$
MAR + SAR	$y = 25.85\ x^{-0.64}$ $r^2 = 0.82$	$y = 31.64\ x^{-0.58}$ $r^2 = 0.70$	$y = 33.30 \log_{10}(x) + 24.88$ $r^2 = 0.57$
NAR + MAR + SAR	$y = 28.98\ x^{-0.66}$ $r^2 = 0.82$	$y = 12.98\ x^{-0.33}$ $r^2 = 0.30$	$y = 40.64 \log_{10}(x) + 11.84$ $r^2 = 0.70$

1479

1480

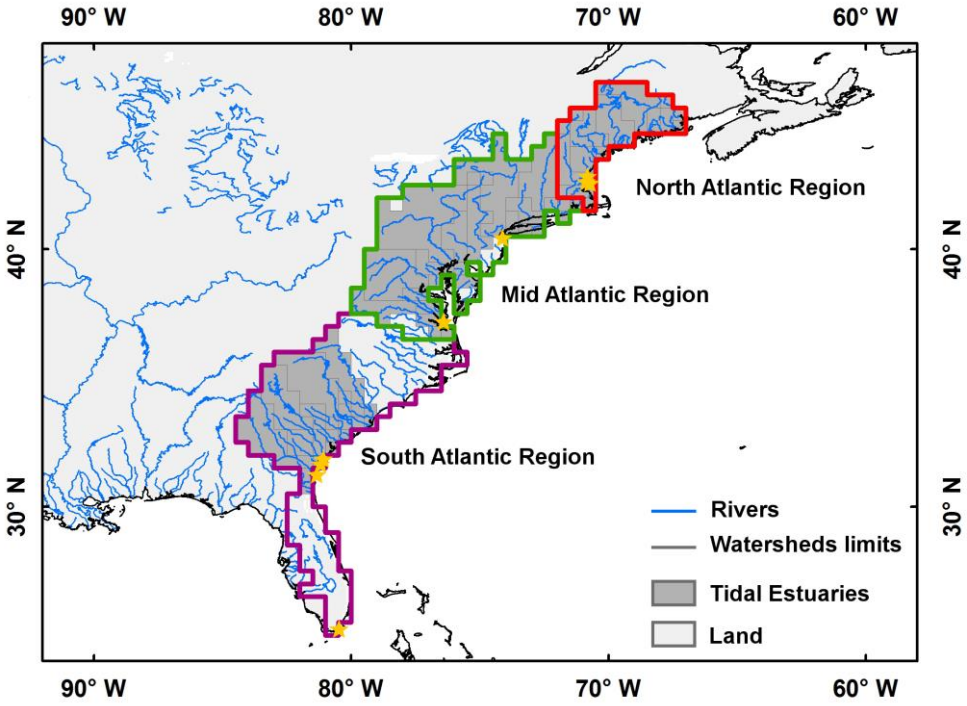

1481

1482 **Figure 1**: Limits of the 0.5 degrees resolution watersheds corresponding to tidal estuaries of the East
1483 coast of the US. 3 sub-regions are delimited with colors and orange stars represent the location of
1484 previous studies.

1485

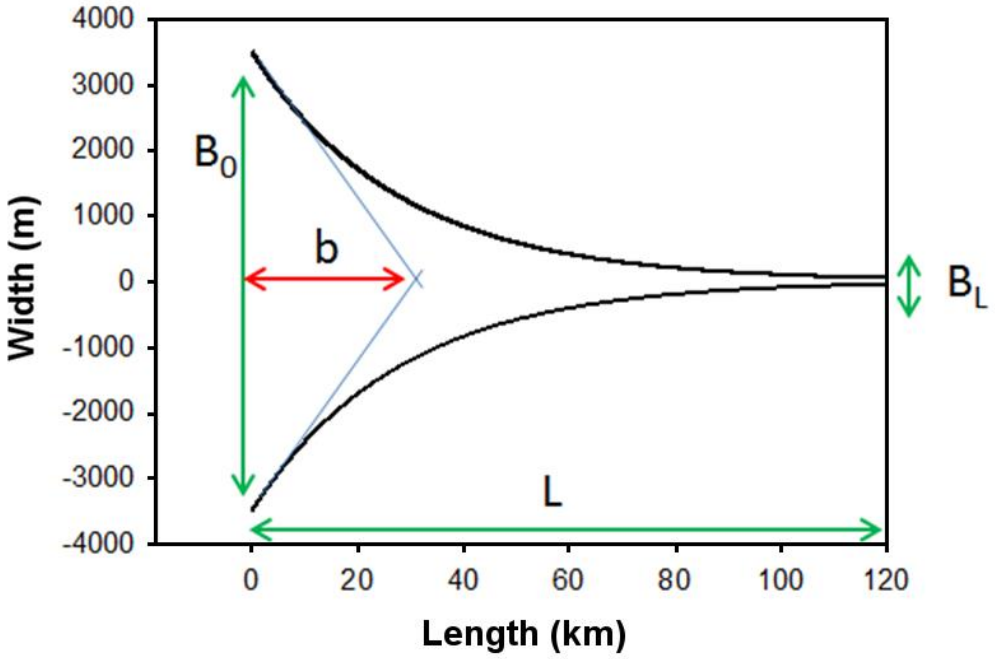

Figure 2: Idealized estuarine geometry and main parameters. Parameters indicated by green arrows are measured, b is calculated. See section 2.3.1 for further details.

1490

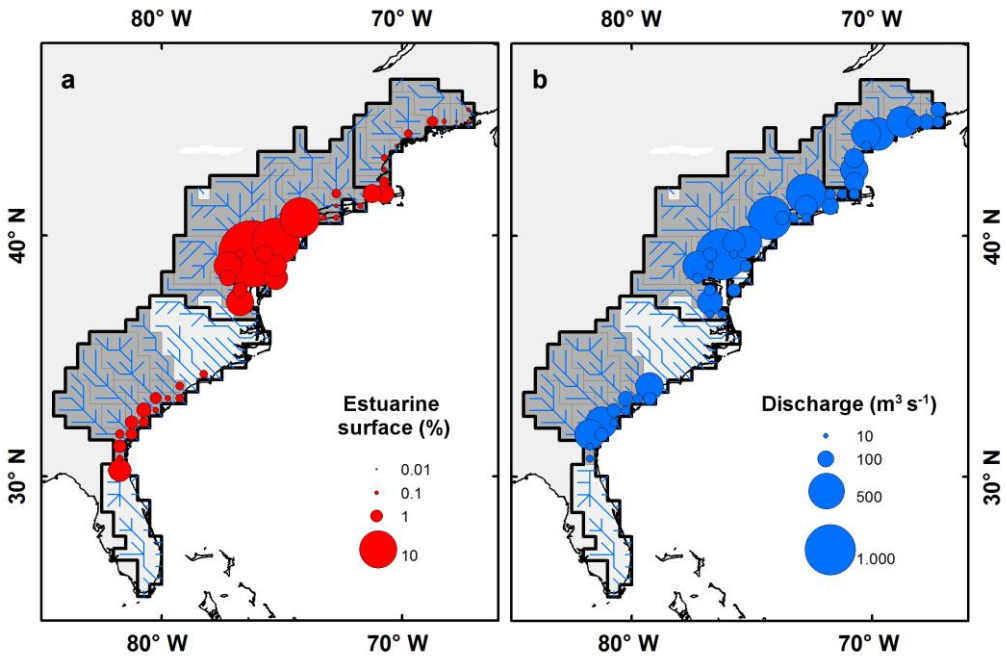

1491

1492 **Figure 3:** Estuarine surface area (a) and mean annual freshwater discharge (b) for each tidal estuary
1493 of the East coast of the US. Estuarine surface area are expressed as percentage of the entire surface
1494 area of the region (19830 km^2)

1495

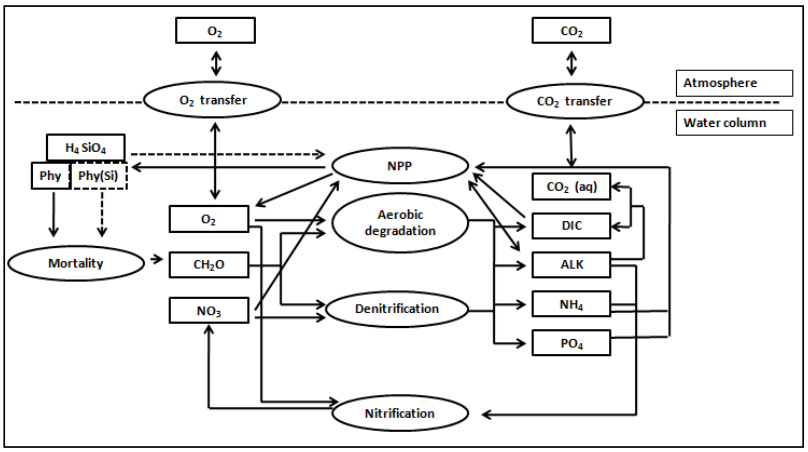

Figure 4: Conceptual scheme of the biogeochemical module of C-GEM used in this study. State-variables and processes are represented by boxes and oval shapes, respectively. Modified from Volta et al., 2014.

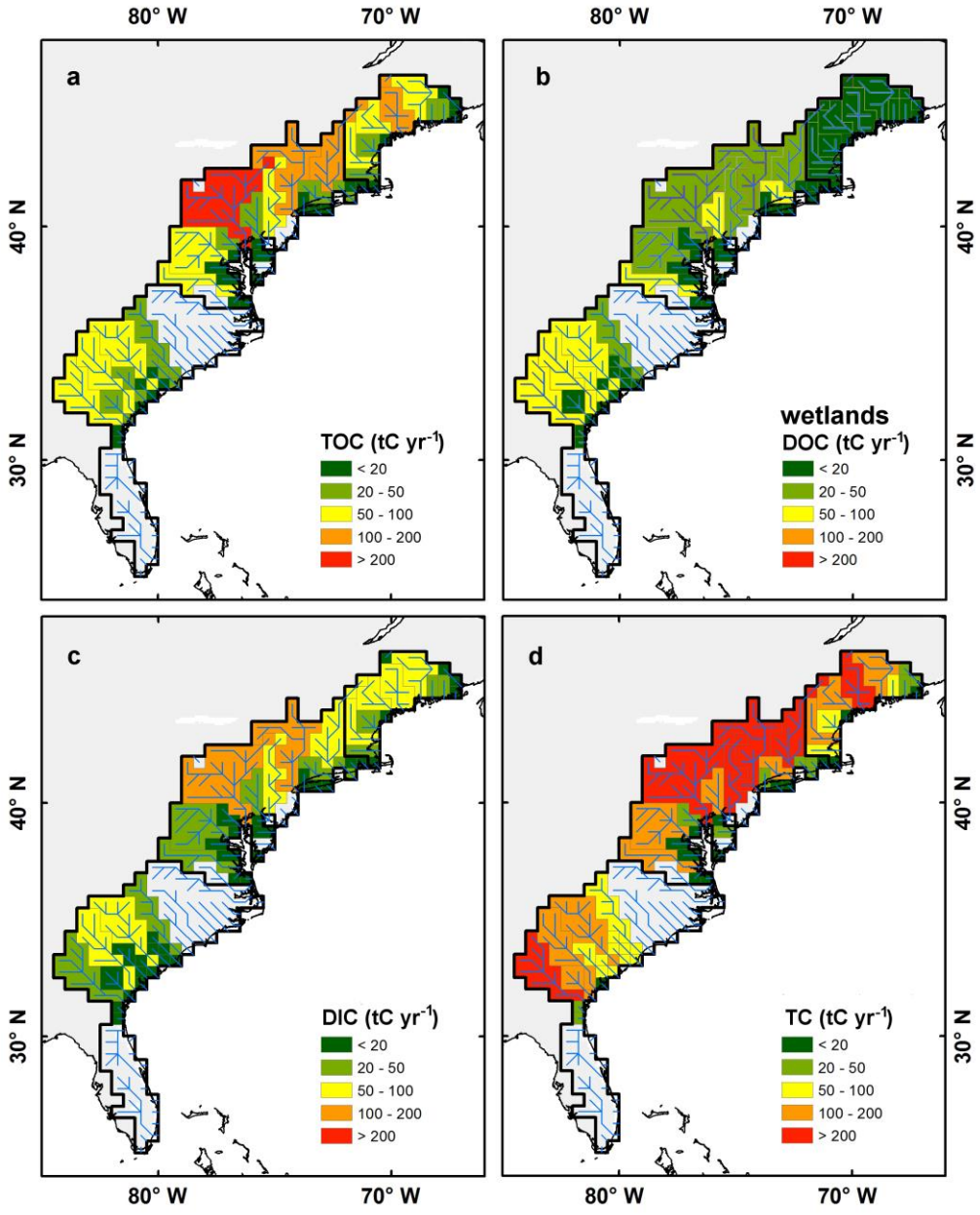

1501

1502 **Figure 5:** Annual river carbon loads of TOC (a), annual DOC fluxes from wetlands (b), annual river
1503 carbon loads of DIC (c) and annual TC fluxes (d). All fluxes are indicated per watershed.

1504

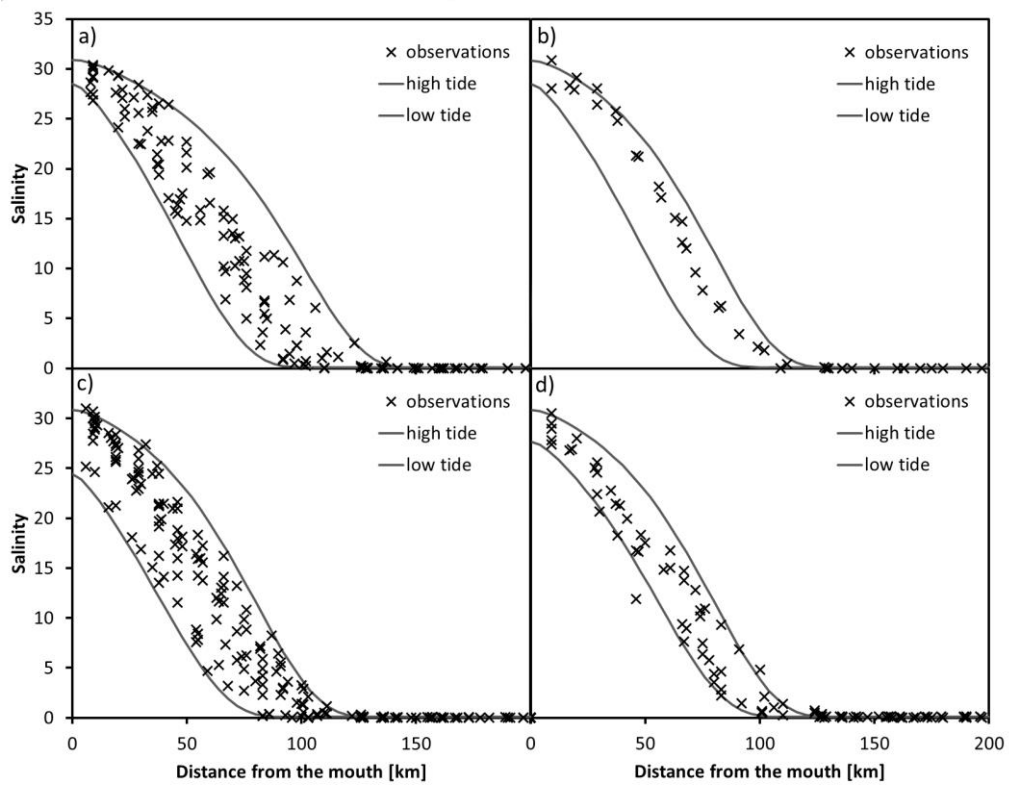

Figure 6. Modeled (lines) and measured (crosses) salinities in the Delaware Bay estuary for January (a), February (b), May (c), June (d). The two lines correspond to high and low tides.

Formatted: Font: Bold, Not Italic

Formatted: Font: Not Italic

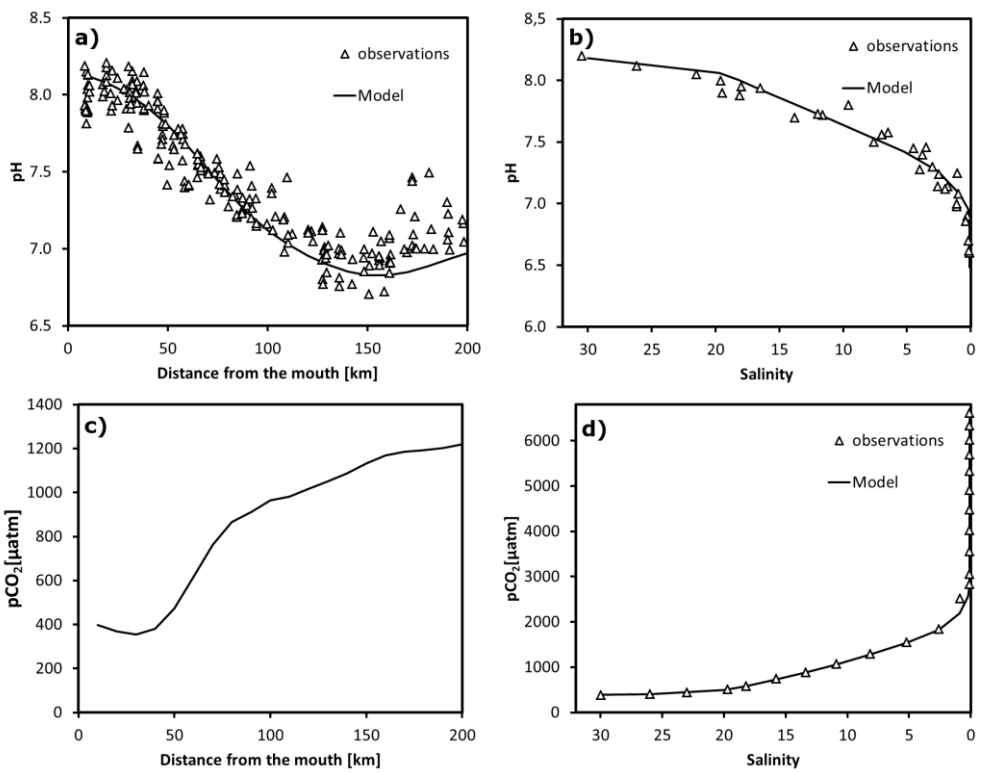

Figure 7. Longitudinal profiles of pH (top) and pCO_2 (bottom) for the Delaware Bay (left) and Altamaha river estuary (right).

Formatted: Font: Not Italic, No underline

Formatted: Font: Not Italic, No underline

Formatted: Font: Not Bold, Not Italic, No underline

Formatted: Font: Not Italic, No underline

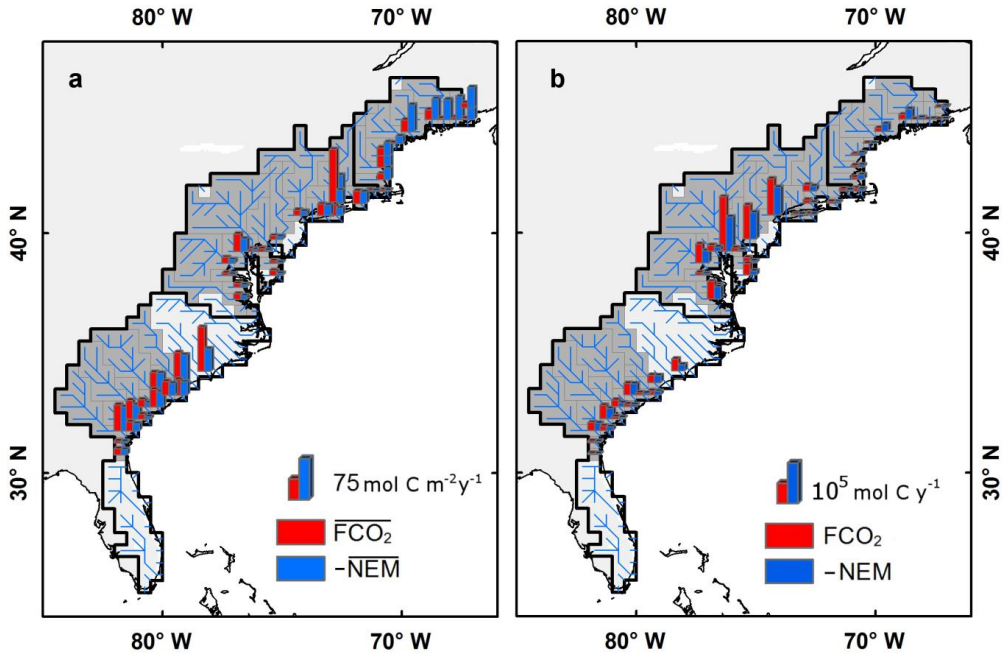

Figure 8: Spatial distribution of spatially averaged value (a) and integrated value (b) of mean annual FCO_2 (red) and -*NEM* (blue) along the East coast of the US. On panel a, the notation with overbars ($\overline{FCO_2}$ and $-\overline{NEM}$) represents rates per unit surface. For the sake of the comparison with $\overline{FCO_2}$, Fig. 8 displays $-\overline{NEM}$ because the model predicts that all estuaries in this region are net heterotrophic.

Deleted: 6

Deleted: figure

Deleted: 6

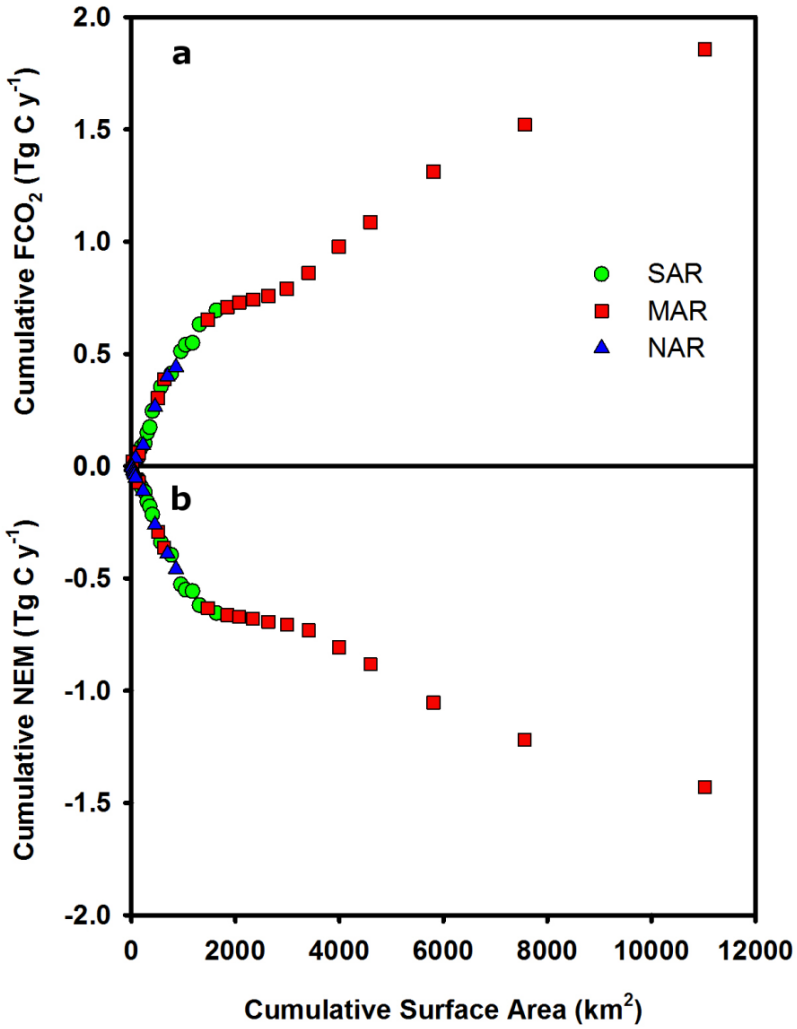

1523

1524 **Figure 9:** The Cumulative *FCO_2* (a) and *NEM* (b) as functions of the cumulative estuarine surface area.
1525 Systems are sorted by increasing surface area.

Deleted: 7

1526

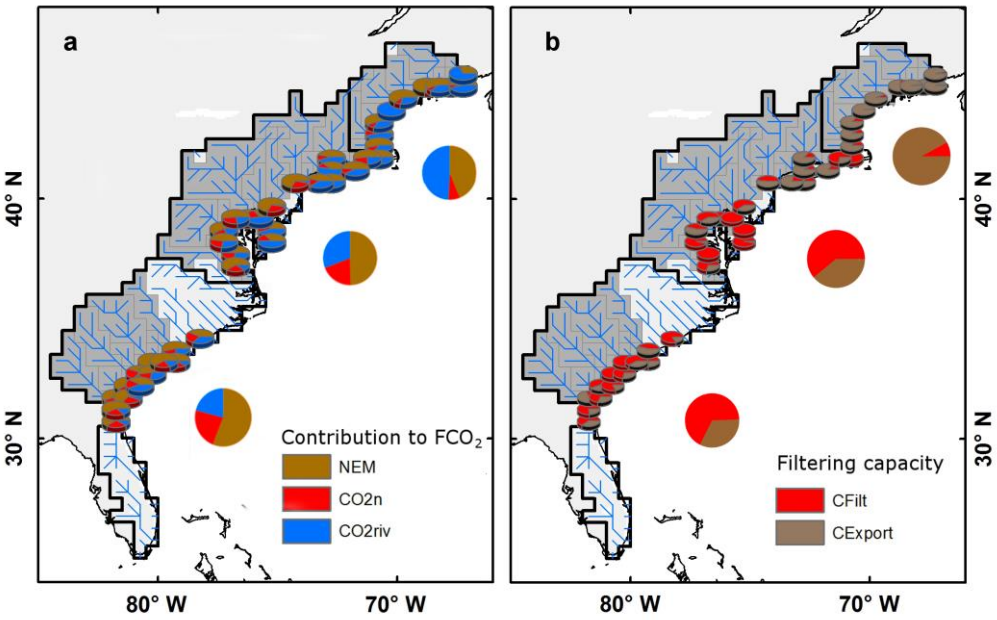

1528

1529 **Figure 10:** Contribution of *NEM*, nitrification and riverine waters super-saturated waters to the mean
1530 annual FCO_2 (a). Spatial distribution of mean annual carbon filtration capacities (*CFilt*) and export
1531 (*CExport*) along the East coast of the US (b).

1532

Deleted: 8

a) Eastern US coast

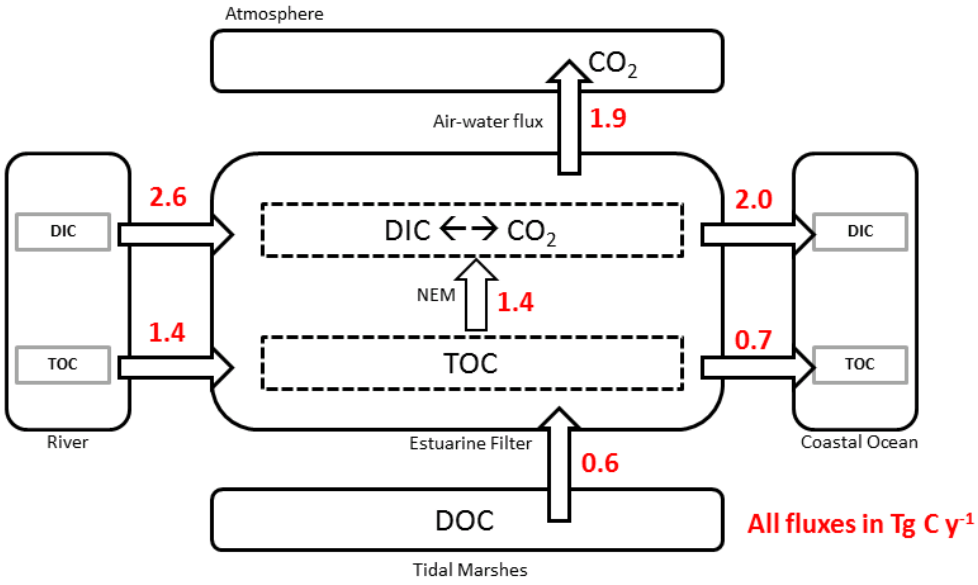

b) North Sea coast

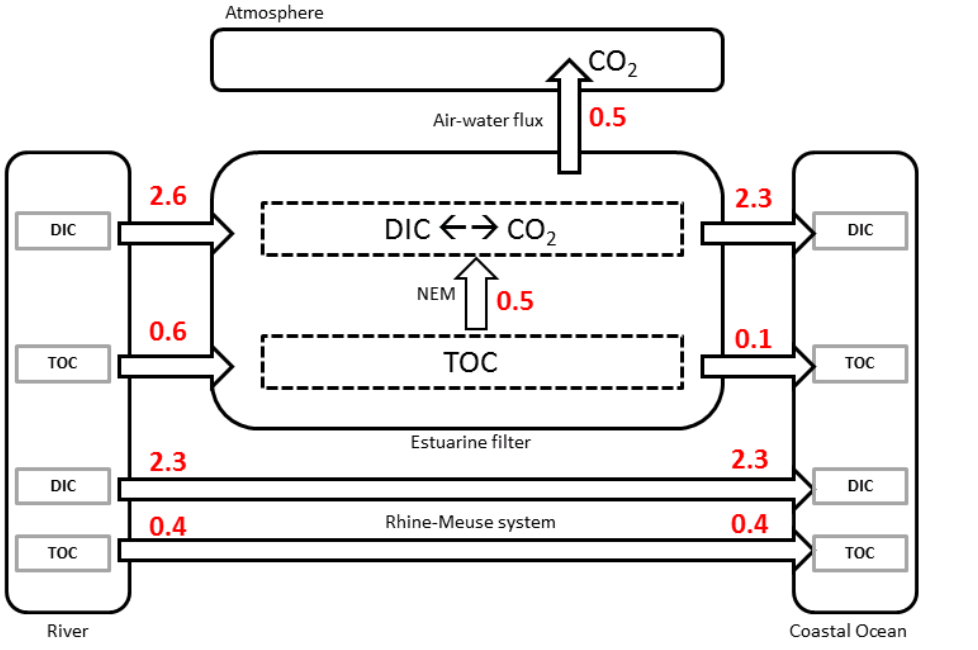

Figure 11: Annual carbon budget of the estuaries of the East coast of the US (a) and of the coast of the North Sea (b, modified from Volta et al., 2016a).

Deleted: 9

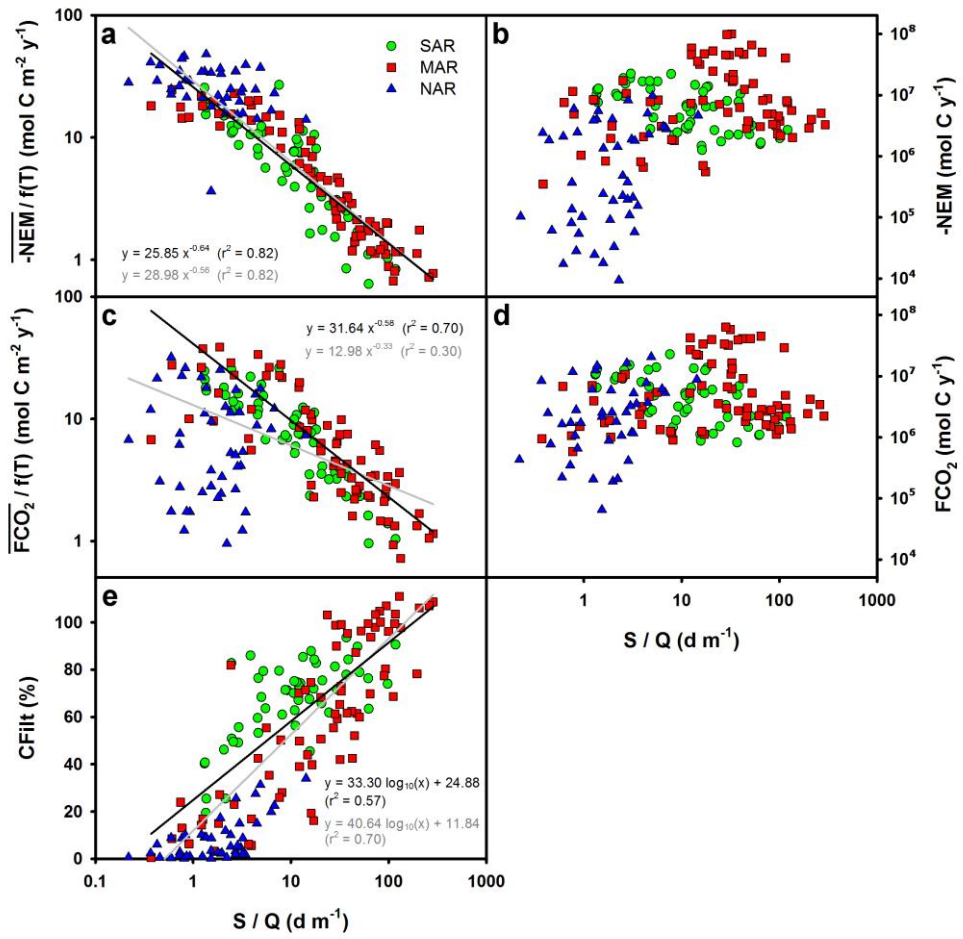

Figure 12: System scale integrated biogeochemical indicators expressed as functions of the depth normalized residence time expressed as the ratio of the estuarine surface S and the river discharge Q for all seasons. Panels b, d and e represent NEM, -FCO_2 and CFilt, respectively. Panels a and c represent NEM, -FCO_2 normalized by a temperature Q_{10} function. Black lines are the best fitted linear regressions obtained using all the point. Grey lines are best fit using only the estuaries from the MAR and SAR regions.

Deleted:

Deleted: 10

Deleted: $-\overline{NEM}\,/\,f(T)$ (a), -NEM (b), $\overline{FCO_2}\,/\,f(T)$ (c), FCO_2 (d) and *CFilt* (e)

Formatted: Font: Not Bold, Not Italic, No underline

Formatted: Font: Not Bold, Not Italic, No underline

Formatted: Font: Not Bold, Not Italic, No underline

Formatted: Font: Not Bold, Not Italic, No underline

Formatted: Font: Not Bold, Not Italic, No underline

Formatted: Font: Not Bold, Not Italic, No underline

Deleted: The grey and black lines are the best fitted regressions obtained using all the point or only the estuaries from the MAR and SAR regions, respectively.